EFDA–JET–PR(12)32

F. Romanelli
and JET EFDA contributors

Overview of the JET Results with the ITER-Like Wall

Overview of the JET Results with the ITER-Like Wall

F. Romanelli
and JET EFDA contributors*

JET-EFDA, Culham Science Centre, OX14 3DB, Abingdon, UK

** See annex of F. Romanelli et al, "Overview of JET Results", (24th IAEA Fusion Energy Conference, San Diego, USA (2012)).*

Preprint of Paper to be submitted for publication in
Nuclear Fusion

ABSTRACT

Following the completion in May 2011 of the shutdown for the installation of the beryllium wall and the tungsten divertor, the first set of JET Campaigns have addressed the investigation of the retention properties and the development of operational scenarios with the new plasma facing materials. The large reduction of the carbon content (more than a factor ten) led to a much lower Z_{eff} (1.2–1.4) during L- and H-mode plasmas, and radiation during the burn-through phase of the plasma initiation with the consequence that breakdown failures are almost absent. Gas balance experiments have shown that fuel retention rates with the new wall are in line with the ITER needs. The re-establishment of high-confinement scenarios compatible with the new wall has required an optimization of the control of metallic impurity sources and heat loads. Stable type I ELMy H-mode regimes with $H_{98,y2}$ close to 1 and $\beta_N \sim 1.6$ have been achieved in high triangularity plasmas. The ELM frequency is the main factor for the control of the metallic impurities accumulation. Pedestal temperatures tend to be lower with the new wall, leading to somewhat reduced confinement, but nitrogen seeding restores high pedestal temperatures and high confinement. Compared with the carbon wall, major disruptions with the new wall show a lower radiated power and a slower current quench. The higher heat loads on plasma-facing components due to lower radiation, made the routine use of massive gas injection for disruption mitigation essential.

1. INTRODUCTION

ITER has adopted beryllium as first wall and tungsten as divertor armour material, to reduce the tritium inventory an order of magnitude below that observed with carbon plasma-facing components (PFC) [1]. JET has been upgraded through a number of projects [2] in order to address the engineering, physics and technology aspects of plasma operation in this new all metal combination and to provide the basis for the effective exploitation of ITER. The JET ITER-like Wall (JET-ILW) [3] was achieved by a full replacement of the pre-existing carbon JET PFCs (JET-C) with the combination of materials foreseen for ITER. The work was completed during a major shutdown which started in October 2009 (Fig.1).

Remote handling was used almost exclusively to remove the existing components and install the 2880 new assemblies. Replacement of the PFCs was complemented by enhancements in Real-Time systems for wall temperature monitoring and plasma control, the latter designed to ensure adequate protection of the new wall. The Neutral Beam Heating (NBI) was upgraded from 20MW/10s pulse to 30MW/20s pulse routine operation and a High Frequency Pellet Injection (HFPI) system for plasma fuelling and ELM control studies was installed. A suite of new diagnostics comprising a sophisticated camera arrangement to be used for real time control was also developed.

Plasma operation was re-established in August 2011 and since then the JET programme has been devoted to investigation of plasma-wall interactions, material migration and retention properties of the ILW in addition to the study of ITER operational scenarios with the new wall (Fig.2) [4].

In section 2 we give an overview of all major engineering and operational results obtained with

the ILW and the implications for ITER operation. In section 3 the development of ITER relevant scenarios in the new all-metal environment is presented, along with confinement and edge pedestal physics results. Conclusions and perspectives are presented in section 4.

2. OPERATION OF JET WITH THE ITER-LIKE WALL.

2.1 PLASMA IMPURITY CONTENT AND IMPURITY SOURCES FROM PLASMA FACING COMPONENTS

From the very first JET-ILW plasmas the impurity content has been significantly reduced as compared to JET-C conditions. The carbon content is on average a factor 20 lower than in comparable JET-C plasmas as taken by the normalised intensity of CIII (97.7nm) line (Fig.3).

Monitoring pulses with constant conditions throughout the campaigns enabled a follow-up on the Wall and impurity evolution. The temporal evolution of the C content in the plasma was documented by optical spectroscopy in monitoring discharges which revealed three phases: an initial clean-up phase, a constant phase, and at the end of campaign a phase with slight increase of C with auxiliary power [5]. However, the carbon flux in the plasma edge – a key parameter for the long term retention in JET-C was reduced by at least a factor 10 throughout the first year of operation with the JET-ILW. A trend towards increased Carbon emissions in the later phases of the JET-ILW campaigns can be attributed to the increase in power and performance of the discharges increasing the core plasma temperature and hence the slightly higher emission observed.

In fact, here is no evidence of any significant increase in residual carbon in time, indicating that no damage of the W-coatings on CFC substrate in the divertor has occurred. Oxygen levels are also lower by roughly one order of magnitude with respect to JET-C with non-optimal wall conditions (although only marginally lower than in JET C-wall plasmas with well conditioned wall and following Be evaporations). The lower residual carbon and oxygen level in JET-ILW is thought to be mainly due to gettering burying of carbon and oxygen by beryllium [7].

This large reduction of residual impurity levels is similar to that found earlier by AUG when going from all-C to a boronised [6] all W-wall. As a consequence the line averaged Z_{eff} typically decreases from 1.5-2.5 (JET-C) to 1.2-1.4 (JET-ILW) for similar values of density and heating power (Fig.4).

Specific effort has been devoted to investigate the impact to the operational space due to W core accumulation [8,9] and surface melting [10]. Beryllium erosion can shorten component lifetimes, contribute to tritium retention by re-deposition [11] and cause significant sputtering of tungsten. Tungsten sputtering has been studied in L- and H-mode discharges.

It is found that for the present range of temperatures and impurity content at JET most of the W sputtering in L-mode can be attributed to low Z impurities, more specifically Be ions (Fig.5).

Experiments in L-mode have been performed to compare the impurity content under neutral beam (NBI) and Ion Cyclotron Resoance Frequency (ICRF) heating. As shown in Fig.6, the bulk radiation, defined as power radiated from inside the separatrix, is higher with ICRF [12] although

significant electron heating is obtained and the increase in plasma energy is similar to C-wall values. It was estimated that around 80% of the radiation comes from W and 20% by Nickel with sources from the divertor entrance and main chamber [13] [14].

The cause for this increased radiation remains the subject of ongoing investigation [12]. In H-mode plasmas, measurements of intra and inter ELM radiation from WI lines [15] indicate that ELM events dominate the sputtering of W (Fig.7).

2.2 PLASMA BREAKDOWN AND CURRENT RAMP-UP

The strong decrease of carbon content in the machine with the ILW has lead to a significant reduction of radiation during the burn-through phase of the plasma initiation. In figure 8 [16], the radiated power as a function of line-integrated density at the end of the burn-through phase is shown for JET-ILW and JET-C data. Breakdown conditions have been studied and optimised in dedicated experiments. The on-axis electric field parameter space has been thoroughly explored and non-assisted breakdown has been routinely demonstrated down to the values expected in ITER (<0.35V/m).

In contrast to plasma restarts with JET-C, a 1MA/15s plasma discharge was easily obtained at the first attempt during the restart. No failed breakdowns attributable to conditioning issues (with applied electric fields in the range of 0.27–1.6V/m) have been observed so far with the ILW. Furthermore, the JET-ILW experience shows no need for glow discharge cleaning or beryllium evaporation to improve wall conditions and facilitate plasma initiation.

The measured duration of the avalanche phase is found to follow the scaling for a Townsend avalanche process [17]. This phase of the breakdown process is dominated by the pre-fill gas and details of the error fields in the vessel, and not affected by the plasma-facing material.

The plasma-facing material had however a strong impact on the burn-through phase of the breakdown. After the avalanche phase the main trend is that the density (and similarly the recycling or D_α intensity) scales with the pre-fill pressure. This is especially true for the ITER-like wall breakdown and highest densities are obtained for the highest pre-fill pressures.

Although common with the C-wall, no breakdown failures due to de-conditioning events, such as disruptions, happened with the ILW [16,17]. Lower radiation at higher electron densities was achieved, making the breakdown more robust. The lower recycling with the ITER-like wall also required additional pre-fill, improved control and fuelling right after breakdown to maintain the density. A model of plasma burn-through has been developed integrating the breakdown, plasma burn-through phase, the ramp-up of plasma current up to the flat-top and for the first time plasma-surface interaction effects [19]. Impurity levels during the breakdown in this model are self-consistently determined by the plasma-surface interactions. These are determined via the impurity sputtering yields and it assumes an exponential decay model of the deuterium recycling coefficient. The rate and power coefficients in the Atomic Data and Analysis Structure (ADAS) package are adopted to solve energy and particle balance. Neutral screening effects are taken into account according to particle species, and the energy and particle balances are calculated. The results show good

agreement with both C and ILW JET data.

The impact of the ILW on the plasma current (IP) diffusion during the IP rise was studied in a series of experiments [20]. Plasmas with early X-point formation showed that during current ramp-up the temperature profile becomes hollow in the centre and lasts until the flat top phase. As a consequence the plasma develops a negative magnetic shear profile in contrast with similar shots in the JET-C. In shots with increased electron density and higher central temperature a higher plasma inductance (li) is obtained as a result of increasing ne during the limiter phase, indicating that the current density profile at that time becomes relatively more peaked. A lower li (matching that of JET-C plasmas) can be recovered at the end of the IP rise by adjusting ne. Adding ICRH (1MW) resulted in a peaked Te profile. These shots showed weak positive shear by the time of the IP flattop, indicating that the required q-profiles for hybrid and advanced scenarios on JET-ILW can be recovered.

2.3 FUEL RETENTION

One of the crucial operational and safety requirements for ITER is to keep the in-vessel tritium inventory within defined limits [21]. This requirement led to the choice of a Be wall and a W divertor on ITER. In order to achieve this, the corresponding retention rate in JET D plasmas should be below ~ 1020D/s. The retention of D with the ILW has been investigated in JET via controlled experiments for several main plasma scenarios and compared with the retention in reference JET-C discharges. The gas balance takes into account the amount of injected D through the gas injection systems and, if applicable, the neutral beam injection, and the number of actively pumped neutrals by the torus pumping systems. The pumped gas is collected by the JET active gas handling system (AGHS), quantified via calibrated pressure measurements (within a precision of 1% [22]), and analysed by gas chromatography; the quantification is currently limited to 2600 Pam3. All experiments were carried out in series of comparable repetitive discharges with minimum 9 and maximum 34 consecutive plasmas, until the number of injected particles reaches approximately the analysis limit of the AGHS which minimises the impact of history effects and maximise the plasma exposure.

The gas balance experiments covered three confinement regimes, L-mode discharges (P_{aux} = 0.5MW), type-III ELMy H-modes (P_{aux} = 5.0MW), and type-I ELMy H-mode plasmas (P_{aux} = 12.0MW) and were executed at a plasma current of I_p = 2MA, a toroidal magnetic field of either B_t = 2.0T or 2.4T with a triangularity $\delta = 0.2$ and $\delta = 0.4$, respectively, covering different injection rates. The D retention as a function of discharge type is presented in Fig. 9 [23].

In comparison to JET-C a drop of the retention rate normalised to the operational time in divertor configuration has been observed for all the three cases: L-mode from $1.27\times10^{21}Ds^{-1}$ down to $4.8\times10^{19}Ds^{-1}$, type-III ELMy H-modes from $1.37\times10^{21}Ds^{-1}$ down to $7.2\times10^{19}Ds^{-1}$ and type-I ELMy H-modes from $1.97\times10^{21}Ds^{-1}$ down to $16\times10^{19}Ds^{-1}$.

In comparison to JET-C the overall reduction in D retention in JET-ILW is at least tenfold, matching well the predictions [11]. The retention of D in the ILW is most likely due to co-deposition

in Be layers. This seems to agree with the relatively high Be influx measured at the divertor inner leg where the D co-deposition is expected to be higher.

In order to have an independent determination of the fuel retention, a final campaign was performed comprising of 151 identical H-mode discharges (2500 plasma seconds NBI–11MW/6s, $Z_{eff} = 1.2$) resulting in a divertor fluence of 5.25×10^{26} Dm^{-2}, equalling roughly one quarter of the divertor fluence of an ITER pulse at full performance [24]. The removal of some ILW tiles is just starting and will be subjected to surface analysis during the next months.

For the JET characteristic exposure times (≈10s), JET-ILW shows a very reproducible dynamic fuel retention which is about 2-2.5 larger than JET-C with a negligible memory effect from previous plasma loading conditions [25]. Typical retention up to the end of discharge is $1.5\text{-}3\times10^{22}$ D with short term excursions above 10^{23} D. The outgassing phase after the discharge recovers the initial wall retention and in time reduces it further. However, this dynamic retention characteristic is sufficient to provide wall pumping in the start up phase of ITER.

Scaling the absolute JET-ILW retention rates to ITER using the same assumptions applied to the original ITER calculations [11] is work in progress but the relative change with respect to an all carbon machine is consistent with ITER expectations.

2.4. DENSITY LIMIT AND DETACHMENT

Tokamak operation at high density with detached divertor is a key element of the current ITER baseline design. Detached divertor operation is mandatory to reduce the heat loads on the divertor target plates down to an acceptable level.

L-mode density limit experiments [26] and modelling [27] with the ILW have been performed at comparable plasma parameters over a wide set of reference JET-C reference, at B_T ~3.0 T, I_p = 2.0MA and ranging from purely ohmic to NBI heated conditions in both low- and high-triangularity magnetic configurations. In JET-ILW and in JET-C, the power radiated in the Scrape-of-Layer (SOL) and divertor increased quasi-linearly with the edge density. The saturation in radiated power for the JET-ILW occurs just below the density limit for detachment (Fig.10a) and is consistently lower (up to 50%) in JET-ILW than in JET-C (Fig.10b). In both cases the density limit occurred at a radiated power fraction (SOL+divertor) of about 50% of the total input power, and at about 20% lower density for the JET-C. The detachment occurred at 30% higher density in JET-ILW than in JET-C (Fig.10c and Fig.10d). At matched input power the difference in the rollover density between the two materials configurations are likely to be somewhat smaller. The ILW has a substantial effect on the electron density and temperature at both strike points as well as on the detachment onset. In the JET-ILW, detachment in the inner and outer divertor legs occurs nearly simultaneously indicating a much smaller in-out divertor asymmetry.

The experimental profile data collected along the divertor confirms the above observations in that the change in the main radiating species and the overall reduction in total radiation in JET-ILW has raised the L-mode disruptive density limit by up to 30-40% (Fig. 11) in all magnetic configurations,

including the ITER relevant vertical target configuration. In addition, significantly higher gas dosing rates (>10^{22} D/s) are needed to reach such limit in the JET-ILW than with the C wall.

The density limit with strike points on the vertical divertor targets where comparable (within 10%) to the horizontal configuration, However, the divertor plasmas greatly differ in these two configurations. The neutral pressure in the sub-divertor region and the integrated Balmer-α emission across the outer divertor leg is 3-4 higher in the vertical configuration than in the horizontal one (which requires 3-4 higher fuelling rates to achieve the same density). Conversely, the vertical configuration is significantly better pumped than the horizontal configuration. Observations show that X-point MARFE formation is more likely to occur in the vertical configuration with a lifetime much longer for JET-ILW (200 ms) than for JET-C. Such longer emissions give the opportunity for testing feedback control schemes for stable fully-detached divertor operation.

Simulations with the edge code package EDGE2D/EIRENE [28,29,30] predict a 50% reduction of the radiated power in the SOL, qualitatively consistent with the measurements. For both wall materials the simulations show the rollover of the divertor ion current at intermediate densities and steady decrease when increasing the upstream density beyond that: the rollover is less pronounced in JET-C as observed experimentally. Key to obtaining these simulation results is the inclusion of additional reaction rates relating to deuterium molecules and molecular ions. However, the simulations underestimate the radiated power in the SOL, and in particular the radiated power in the divertor, independent of the materials configuration. The predicted power conducted to the outer divertor target is, however, within the uncertainties and limitations of the measurements. For a corresponding vertical configuration and the same upstream conditions as in a horizontal configuration, the simulations predict up to an order of magnitude lower electron temperature at the separatrix and on the outer divertor target, as observed in previous calculations [31].

2.5 DISRUPTIONS

In Fig. 12 is depicted the comparison between JET-C and JET-ILW of several relevant quantities measured during a disruption [32]. The observed reduced radiation has important consequences for the timescales of the disruption process and its impact on PFCs. Higher plasma temperatures after the thermal quench, up to 1 keV, are observed in JET-ILW with a current decay time significantly longer than in JET-C. With the carbon wall, about 80% of all unmitigated disruptions had a linear normalised current quench time below 6ms/m^2. With the JET-ILW only 15% are in that range and 20% have a very long current quench well above 20ms/m^2. Due to the slow current quench higher halo fractions (up to 40%) are more likely to occur [17].

Because of the lower radiation a larger fraction of the energy is conducted to the PFCs for unmitigated ILW disruptions. Temperatures close to Be melting point (1278 °C) have been measured by IR cameras, with some local melting being detected by subsequent visual inspection.

In order to mitigate the higher forces and heat loads, the use of real-time massive gas injection (MGI) became essential to the operation of JET. The use of MGI [18][32][33] has been extremely

successful in mitigating disruptions in high-current H-modes up to 3.5MA. The energy radiated during a disruption for the JET-C and JET-ILW is presented in Fig.13. The fraction of energy radiated during disruptions has dropped from 50-100% for JET-C down to 10% -50% for JET-ILW. However the use of MGI allows recovering the radiation fraction similar to the JET-C.

In JET-C the reaction of the vessel was found to scale proportionally to the halo current [34]. In the JET-ILW the reaction force or vessel displacement was found to vary with the magnitude of the force due to the halo current, as shown in Fig. 14, but also with the impulse (i.e. the time integrated force). Hence, the longer current quench duration also led to larger impulses and thus larger reaction forces on the vessel. Again, the use of MGI allows to convert most of the current quench energy into radiation damping the reaction forces in the vessel.

2.6. PLASMA FACING COMPONENTS POWER HANDLING AND PROTECTION

The design of the ILW components has taken into account plasma operation at high power (NBI 35MW and ICRF 5MW) and high plasma current (disruptions up to 6 MA). A completely new design was required due to constraints on the size of the tiles because of eddy currents and thermal and electromechanical stresses. The Be tiles are made up of blocks mounted in an Inconel carrier with a castellated plasma-facing surface and cuts to reduce the area of eddy current loops [34]. In addition, the tile profiles were optimised to maximise the power handling (Fig.15) and no leading edges above 40mm effective height are exposed in high heat flux areas [35].

The thermal properties of the new wall materials results in new limits for heat loads to PFCs. The Be tiles are at risk of melting, rather than sublimating as CFC tiles, at lower wall temperatures (1278°C). In the divertor, the main risk for bulk W components is thermal fatigue induced cracking while for the W-coated CFC tiles the main limit is posed by carbidisation and inter-layer embrittlement. Thus, the limit for the surface temperature of the divertor components during the initial ILW campaigns was set between 1000–1200°C. An integrated protection of the ITER-like wall (PIW) was implemented. It comprises of CCD cameras, operating in the near infra-red and covering up to 66% of the PFCs and 43% of the divertor, linked to a Real-Time system connecting all main tokamak controls and heating systems [36]. Detection of high temperatures in one or more of the monitored regions triggers a tailored response, ranging from decreasing additional heating power, to changing the magnetic configuration and, in extreme cases, to the orderly termination of the plasma pulse. In the area covered by the CCD cameras no melt damage to the main JET limiters and no unexpected hot spots on the inner and outer wall limiter surfaces have been observed. A single small melt spot on a limiter (Be) was caused by a runaway electron beam created during an emergency stop at the start of the campaign when the protection system was being commissioned. Two inner wall limiters have been found damaged in areas hidden from the protection cameras. The unexpected toroidal asymmetry which caused this could be compounded by a steepening.of the power profile observed near the last closed flux surface. This observation may be related to the funnel effect [37] which was not taken into account in the ILW design and is therefore relevant to optimisation of the ITER limiters.

Dedicated experiments have been carried out to verify the power handling limits set by the bulk W divertor with its lamella structure [38] and geometry. The bulk W divertor was designed to withstand loads up to 9MW/m^2 for a total conducted energy of 60MJ/m^2 and a maximum surface temperature of 2200^{o}C. Plasma operation with conducted energies of ~30MJ/m^2 has been performed routinely keeping the tile surface temperature below 1000^{o}C and the supporting structure below 360^{o}C. Conducted energies up to ~48MJ/m^2 have also been applied where the surface temperature reached ~1200^{o}C. Overall the bulk W tile has achieved the technical design requirements and no damage has been observed. The experience gained with the JET-ILW PFCs design is of high relevance to the ITER design.

3. H-MODE PHYSICS IN ALL-METAL ENVIRONMENT

The qualification of the ELMy H-mode and of the hybrid regime with the ILW has provided a number of results of direct relevance for ITER.

3.1. L-H POWER THRESHOLD

A set of reference JET-C discharges was selected for L-H power threshold studies and closely matching JET-ILW discharges have been produced. In the reference JET-C discharges the L-H power threshold, Pthr, was found to be consistent with the multi machine ITPA scaling law [39] down to very low densities of 1×10^{19} m^{-3} [40], where previous JET-C experiments with the MkII-GB septum divertor had shown deviations from the scaling [41][42] at low plasma density (higher power required). For JET-ILW the L-H power threshold is found to differ both in magnitude and in its dependence on the plasma density compared to the reference JET-C discharges, as shown in Fig.16 [43]. Pthr is reduced by ~ 30% at higher densities (>2×10^{19} m^{-3}), while it increases below a minimum density (~2×10^{19} m^{-3}) thus recovering the low density behaviour first observed with the earlier MkII-GB septum divertor in JET-C.

These findings apply both to P_{thr} and to the net power crossing the separatrix (namely, after subtraction of the core radiation the ICRH values practically overlap the NBI values). In addition, the minimum density $n_{e,min}$ and the minimum H-mode access power are found to increase roughly linearly with magnetic field.

A similar reduction in P_{thr} by ~ 25% has also been reported by AUG with W wall [44]. The L-H power threshold in JET-ILW is also sensitive to variations in divertor configuration and main plasma shape [43], features which are not captured in the ITPA scaling law. Comparison of the JET C and ILW dataset with a recently proposed local model for the L-H transition [45] is in progress.

3.2. BASELINE H-MODE SCENARIO

The baseline type I ELMy H-mode regime was re-established with the ILW as soon as sufficient NBI power became available. As mentioned in section 2.1, the early H-mode experiments were affected by metallic impurity influx events, whose occurrence strongly decreased with further operation, suggesting a conditioning effect of the newly installed divertor surface.

By the end of the 2012 JET campaign, the operating space for baseline H-modes had almost recovered the full range of parameters explored with the C wall. H-mode discharges have been produced in both low and high triangularity (d) configurations, mostly with the Inner Strike Point (ISP) on a W-coated vertical target and the Outer strike Point (OSP) on the bulk W tiles. A limited exploration of an ITER-relevant vertical target divertor configuration was, also, carried out. H-modes were produced with total injected power of 25.5MW up to 3.5MA at low δ (Pulse No: 83479). A representative H-mode shot at 2.5MA and 2.7T with H_{98}~0.9 is shown in Fig.17 [46].

As already observed in AUG with the W wall [44], the behaviour of the baseline H-mode was influenced by the change of first wall and divertor materials. In type I ELMy H-modes at relatively low ELM frequency ~10-15Hz, e.g. at low power or low levels of gas dosing, typically < 10^{22} el/s at 2.5MA, the global confinement can transiently achieve H_{98}~1 but the discharge evolution tends to be dominated by W accumulation (Fig.18). W accumulation can be avoided and more stationary conditions can be obtained in H-modes at higher ELM frequencies, using significant amounts (> 10^{22} el/s) of gas dosing and/or higher input power. If the sawtooth activity is not maintained then central W accumulation is more likely to occur (Fig.18). Increasing core density may lead to suppression of W accumulation but at the expense of global confinement. Similarly, in L-mode plasmas the content of W decreases in the core while it increases to the outer target as the density increases and the divertor temperature decreases [47]. As shown hereinafter, application of core ICRH minority heating (up to 4MW) and/or more central NBI deposition have been investigated showing encouraging results for W content control.

The increase of the NBI power combined with strong deuterium gas puffing rate (above 10^{22}D/s) opens up the operating space by increasing the ELM frequency and therefore flushing out tungsten. ELM frequency increases linearly with NBI power and deuterium gas puffing as shown in the Fig.19. While the increase of NBI power enhances the tungsten source and the gas puffing tends to decrease it, it was found that the minimum gas puffing rate decreases with the injected power. In terms of minimum ELM frequency a lower limit of 10Hz was found in all scenarios with an H-mode.

Normalised confinement in baseline H-modes tends to decrease with increasing gas fuelling levels. Similarly to JET-C data, the stationary discharges obtained in JET-ILW with large fuelling, and high density, exhibit confinement in the range $H_{98,y2}$~0.7-0.9. A major difference with respect to JET-C has been identified in high d H-modes plasmas. Their confinement is significantly lower (20-30%) than equivalent JET-C cases and the access to a regime of good confinement at high gas fuelling has not yet been recovered with the JET-ILW.

The lower confinement observed in JET-ILW can be mainly attributed to lower edge pedestal temperatures. The trend is illustrated in Fig.20 [48,49], where the temperature at the pedestal top (T_e-ped) normalised to the plasma current (I_p) is plotted versus the density at the pedestal top (n_e-ped) normalised to the Greenwald density (n_{gw}). A direct comparison of high δ pulses at 2.5MA, with the same power at the separatrix and the same density at the top of the pedestal, shows a reduction of the pedestal electron temperature by 30% (from ~1keV down to ~700eV) in the ILW case, while the profiles inside the pedestal show the same stiffness.

In addition, the type I ELMs in high deuterium fuelling pulses, at low pedestal temperatures, exhibit a much slower crash of the edge electron temperature than similar JET-C cases and, consequently, a slower rise in divertor ELM heat load and reduced surface peak temperatures for a given drop in stored energy.

Infra-red data shows that slow crashes in pedestal temperature measured by ECE corresponds to a slow rise in divertor power and hence much reduced peak temperatures for a given change in stored energy. These 'benign' type I ELMs exist in an edge parameter space which is below the type I / type III ELM boundary for the carbon wall. As depicted in Fig.21a, after the initial 2ms temperature decay there are two classes of ELM, in one type the edge temperature recovers and in the other the decline continues, at a lower rate. Using nitrogen seeding, as shown in Fig.21b, speeds up the ELM crash and makes it more akin to that seen with the carbon wall [50].

Experiments using nitrogen and neon seeding have been carried out systematically in high and low d plasmas. The most interesting results have been obtained in high-δ/2.5 MA plasmas (Fig. 22) [51], where nitrogen seeding has been proven to raise both pedestal density and temperature with respect to un-seeded pulses. In these conditions the maximum confinement recovers to $H_{98,y2}$~0.92, close to equivalent nitrogen seeded pulses in JET-C. With nitrogen seeding the radiated power increases up to ~60% of the input power, cooling the edge plasma and reducing the inter-ELM W source, and the ELM frequency decreases. These plasmas, however, are still somewhat far from stationary conditions and tend to evolve towards behaviour dominated by W accumulation.

While it is obvious that the change in wall composition is at the root of the different baseline H-mode behaviour in ILW, the investigation of the specific effects causing W accumulation at low ELM frequency and low confinement in high d configurations is progressing. Significant variations in core vs. divertor radiation patterns, in impurity content and Zeff as well as in neutral recycling have been identified and their impact on divertor, and core, plasma will be the subject of further analysis.

3.3. HYBRID H-MODE SCENARIO

The hybrid H-mode scenario offers the prospect of extended pulse length and H_{98}>1 at reduced plasma current with respect to the baseline H-mode.

Very promising results were obtained in JET-C and re-development of this scenario in JET-ILW has been an important area of research. The Hybrid H-mode scenario has been re-established in JET-ILW both at low and high triangularity at medium current values, up to 2 MA and input power up to 24.1MW (as in Pulse No: 83328; NBI 23.4MW) [46]. As with the baseline H-modes, the operation range is somewhat restricted by W accumulation in discharges with no gas puffing. The amount of gas fuelling needed to control the W accumulation is, however, less than in comparable baseline plasmas. The discharge shown in Fig.23, with H_{98}~1.2 and β_N~2.8, is well within the typical scatter of results with the carbon wall (best pulses had H_{98}~1.4).

The pedestal pressure is lower in the high delta hybrid plasmas for JET-ILW compared to JET-C and the core profiles are more peaked, resulting in a similar overall confinement [49]. At low d,

similar global confinement to C-wall reference cases is obtained but with higher density and lower temperature. As in AUG with the W wall, optimisation of the central heating has been employed to avoid W core accumulation.

As a general trend for all type of discharges depicted in Fig.24, the confinement in the JET-ILW is lower in the region of $P_{net}/P_{thr,98} < 2$ (where Pnet is the net input power, and $P_{thr,98}$ is the L-H power threshold from Martin scaling [39]) However, when the injected power is increased further to the range $2 < P_{NET}/ P_{thr,98} < 3$ JET-ILW plasmas present a confinement range similar to JET-C, for the same absolute input power around 25 MW. It is important to note the differences between both type of discharges in the data set where hybrid plasmas have $3.5 \leq q_{95} \leq 4.5$ and $\beta \leq 3.5$ whereas the baseline plasmas present $2.8 \leq q_{95} \leq 3.6$ and $\beta \leq 2$ that could be part of the reason for the higher efficiency that hybrids show in confining the thermal energy sustaining a stronger Te profile peaking than the baseline scenarios. This result is in line with the observed slightly improvement of confinement time for a sub-set of discharges (mainly hybrids) with $I_p < 2.1$MA [49].

3.4. ELM CONTROL

JET is equipped with several external methods to control the ELM activity and first experiments have been performed.

The JET High Frequency Pellet Injector (HFPI) [52] was implemented with the major goal to establish ELM pacing in ITER relevant scenarios with negligible fuelling. The particle flux rate for ELM pacing at 50 Hz is expected to be about 1×10^{22} D/s corresponding to a rather low gas plasma fuelling rate. Injection of pacing pellets from the Low Field Side (LFS) had a reliability of 33% due to the design of the pellet track. With about 1/3 of the pellets arriving almost intact to the plasma (with a small scatter in size), it was achieved a pacing efficiency up to 60% was achieved, resulting in an ELM frequency increase from 7 up to 31Hz. Pellets launched from the Vertical High Field Side (VHFS) showed low delivery efficiency from the injection system but significantly higher ELM trigger potential. Fuelling size pellets were injected reliably at 15 Hz with a nominal pellet size of 22×10^{20} D; persistent ELM control was demonstrated in baseline H-mode discharges both with low and high triangularity (Fig. 25).

The JET Error Field Correction Coils (EFCC) are used to produce RMPs for ELM mitigation studies, have been recently upgraded, doubling their coil current capability up to 96kAt. This enhancement expands the applicability of RMP as an ELM control/ suppression mechanism in plasmas with ITER-relevant materials in addition to the results obtained in other devices with different PFCs [53][54][55]. ELM mitigation experiments with magnetic perturbations have been performed at low and high collisionality in JET-ILW Error! Reference source not found.. In the low collisionality JET-ILW plasmas (Fig.26) the use of EFCC for application of $n = 2$ field has the effect to increase the ELM frequency from 20Hz up to 80Hz. This was not observed in the previous JET-C EFCC ELM control experiments, at lower EFCC current. The amount of splitting seems to be linked to the amplitude of the perturbation field and the edge safety factor, q_{95}.

A strong effect on type-I ELMs was observed when a n = 2 field is applied at high collisionality ($\nu^*_e = 2.0$). Type-I ELMs ($f_{ELM} \sim 45$Hz) are replaced by high frequency small ELMs ($f_{ELM} \sim$ few hundreds Hz).

There is no drop in the core electron density and temperature during the application of the n = 2 field, even with EFCC integrated current up to 88kAt. Again, splitting of the outer strike point has been observed during the mitigation of the type-I ELMs. This experimental observation is similar to that observed with an n = 2 field in the high collisionality H-mode plasmas on AUG [54] with a full W wall. In contrast, the impact of the EFCC of an n = 2 field in high collisionality H-mode plasmas in JET-C was almost absent [56].

In addition to pellet pacing and EFCC, ELMs can be triggered at JET by rapid variations of the Radial Field, the so-called Vertical Kicks. This technique was already applied in JET-C H-mode plasmas, demonstrating that ELMs can be synchronised with the imposed kick frequency [57]. In JET-ILW only a limited number of kick experiments has been carried out so far, mostly under cold pedestal conditions typical of the high fuelling ILW H-modes. The experimental results (Fig.27) indicates that full control of the ELM frequency can be obtained up to the maximum value explored of ~42Hz for radial field perturbations sligthly higher than in JET-C. The difference in kick size is likely to be related with the difference in pedestal temperature between the present experiments in the Be/W wall (gas fuelled plasmas, with $T_{e,ped} < 0.6$keV) and the previous ones carried out in JET with the carbon wall (unfuelled plasmas, with $T_{e,ped} \sim 1$keV). Scans of both kick amplitude (radial field circuit), from 3 to 12kV, and duration, from 1.5 to 4.5ms, have been carried out to investigate the physics of ELM triggering by kicks. Initial analysis suggests that the probability to trigger an ELM depends more strongly on the duration than on the amplitude of the kick.

CONCLUSIONS AND PERSPECTIVES

The first year of operation with the JET ILW has provided a number of important results in view of the use of beryllium and tungsten as plasma facing materials in ITER. The expectation of low tritium retention has been confirmed by the large reduction in the fuel retention with respect to a full carbon wall. Operation with beryllium and tungsten are characterized by reduced level of radiation and reliable ITER relevant break-down conditions (<0.35Vm^{-1}). The reduction of radiated power leads to an increase of the thermal loads on PFCs during disruptions and to larger vessel forces. However, the use of massive gas injection has proven to mitigate JET disruptions efficiently up to high plasma current (3.5MA) and it is now routinely used. The development of plasma scenarios has achieved important milestones, with the re-establishment of robust type-I ELMy H-mode and hybrid regimes the latter with confinement 30% above the ITER scaling. High power type-I ELMy H-modes avoid tungsten accumulation due to lower W penetration at increased ELM frequencies (> 10Hz). Pedestal characteristics tends to be different between the ILW and the carbon wall, with lower pedestal temperatures in the present configuration in conditions where the radiation from W is minimal. Nitrogen seeding has been investigated, and has let to increased pedestal temperature similar to AUG.

The ILW exploitation will continue in 2013 with the main aim of demonstrating satisfactory operation in the presence of shallow melting of tungsten by ELMs, in view of the final ITER decision on the use of tungsten. The progressive increase of plasma performance is the objective of the 2014 and 2015 campaigns. In the longer term, preparation of a DT experiment is the main objective.

Following the completion of the feasibility studies for new JET enhancements, the design and R&D activity for a set of internal Resonant Magnetic Perturbation coils is being progressed in collaboration with the Institute for Plasma Research in Gandhinagar with the goal of being ready for a decision on the procurement of the full system by mid 2013.

ACKNOWLEDGMENTS

The results presented in this paper have been obtained by the collective efforts of all JET EFDA contributors, listed in the Appendix, and those working under the auspices of the JET Operation Contract. The author is particularly thankful to L. Horton F. Rimini, G. Sips, G. Matthews, A. Malaquias and to the JET TaskForce Leaders and Deputies. This work was supported by EURATOM and carried out within the framework of the European Fusion Development Agreement. The views and opinions expressed herein do not necessarily reflect those of the European Commission.

REFERENCES

[1]. R. Pitts, et al. Journal of Nuclear Materials,Volume **415**, Issue 1, p. S957-S964.
[2]. J. Pamela, et al. Journal of Nuclear Materials **363–365**, 1 – 11 (2007).
[3]. G.F. Matthews et al., 2009 Physica Scripta **T138** 014030.
[4]. G.F.Matthews, 20th International Conference on Plasma Surface Interactions in Controlled Fusion (Aachen, 2012)
[5]. S. Brezinsek presented at 20th PSI conference 2012
[6]. A. Kallenbach et al. Nuclear Fusion **49** (2009) 045007
[7]. S. Brezinsek et al., 24th IAEA Fusion Energy Conference (FEC2012), San Diego
[8]. T. Pütterich et al., 24th IAEA Fusion Energy Conference (FEC2012), San Diego
[9]. R. Neu et al., Nuclear Fusion **45** (2005) 209
[10]. J.W. Coenen et al., 24th IAEA Fusion Energy Conference (FEC2012), San Diego
[11]. J. Roth et al., Plasma Physics and Controlled Fusion **50** (2008) 103001
[12]. M.H.R. Mayoral et al., 24th IAEA Fusion Energy Conference (FEC2012), San Diego
[13]. T. Pütterich et al., 2008 Plasma Physics and Controlled Fusion **50** 085016
[14]. A. Czarnecka et al., 39th EPS Conference & 16th International Congress on Plasma Physics P5.047 (2012).
[15]. G. van Rooij et al., 24th IAEA Fusion Energy Conference (FEC2012), San Diego
[16]. P.C. DeVries et al., 24th IAEA Fusion Energy Conference (FEC2012), San Diego
[17]. B. Lloyd, et al., Nuclear Fusion **31** (1991) 2031.
[18]. P.C. DeVries et al., 39th European Physical Society Conference on Plasma Physics (EPS2012), Stockholm

[19]. H.T. Kim et al., submitted to Journal of Nuclear Materials (2013)
[20]. J. Mailloux et al., 39th European Physical Society Conference on Plasma Physics (EPS2012), Stockholm
[21]. J. Roth et al., Journal of Nuclear Materials **390–391**, 1–9 (2009)
[22]. R. Lässer et al. Fusion Engineering and Design **47** (1999) 173
[23]. T. Loarer et al., 20th International Conference on Plasma Surface Interactions in Controlled Fusion (Aachen, 2012)
[24]. A. Kukushkin presented at 20th PSI conference 2012
[25]. V. Philipps et al., 20th International Conference on Plasma Surface Interactions in Controlled Fusion (Aachen, 2012)
[26]. A. Huber et al., 20th International Conference on Plasma Surface Interactions in Controlled Fusion (Aachen, 2012)
[27]. M. Groth et al., 24th IAEA Fusion Energy Conference (FEC2012), San Diego
[28]. R. Simonini., et al., Contribution Plasma Physics **34** (1994) 368
[29]. D. Reiter, et al., Journal of Nuclear Materials **196–198** (1992) 80
[30]. S. Wiesen, JET ITC-Report, http://www.eirene.de/e2deir_report_30jun06.pdf (2006)
[31]. A. Loarte et al., Plasma Physics and Controlled Fusion **43** (2001) R183
[32]. M. Lehnen at al., 24th IAEA Fusion Energy Conference (FEC2012), San Diego
[22]. C. Reux et al., 27th Symposium on Fusion Technology (SOFT-2012), Liege
[34]. V. Riccardo et al., 27th Symposium on Fusion Technology (SOFT-2012), Liege
[35]. I.M. Nunes et al., 24th IAEA Fusion Energy Conference (FEC2012), San Diego
[36]. G. Arnoux et al., High Temperature Plasma Diagnostics (HTPD) 2012, Monterey, California
[37]. G. Arnoux et al. 24th IAEA Fusion Energy Conference (FEC2012), San Diego
[38]. Ph. Mertens et al., 20th International Conferenceon Plasma Surface Interactions in Controlled Fusion (Aachen, 2012)
[39]. Y.R. Martin et al., 2008 Journal of Physics: Conference Series **123** 012033
[40]. C.F. Maggi et al., 38th EPS Conference on Plasma Physics, (Strasbourg 2011)
[41]. L.D. Horton et al., 26th EPS Conference on Controlled Fusion and Plasma Physics (Maastricht) 1999
[42]. Y. Andrew et al., Plasma Physics and Controlled Fusion **48** (2006) 479
[43]. C.F. Maggi et al., 39th European Physical Society Conference on Plasma Physics (EPS2012), Stockholm
[44]. R. Neu et al., 20th Int. Conf. on Plasma Surface Interactions in Controlled Fusion (Aachen, 2012)
[45]. W. Fundamenski et al., Nuclear Fusion **52** (2012) 062003
[46]. E. Joffrin et al., 24th IAEA Fusion Energy Conference (FEC2012), San Diego
[47]. S. Brezinsek et al., 39th European Physical Society Conf.on Plasma Physics (EPS2012), Stockholm

[48]. L. Frassineti et al., 39th European Physical Society Conf. on Plasma Physics (EPS2012), Stockholm
[49]. M.N.A. Beurskens et al., 24th IAEA Fusion Energy Conference (FEC2012), San Diego
[50]. M.N.A. Beurskens et al., Nuclear Fusion **49** (2009) 125006
[51]. C. Giroud et al., 24th IAEA Fusion Energy Conference (FEC2012), San Diego
[52]. P. Lang et al., Pedestal and Edge Physics ITPA meeting , Hefei, China
[53]. T.E. Evans et al., et al. Nature ofPhysics **2**, 419 (2006)
[54]. Y. Liang et al., Physical Review Letters **98**, 265004 (2007)
[55]. W. Suttrop, et al. Physical Review Letters **106**, 225004 (2011)
[56]. Y. Liang et al., Nuclear Fusion **50** 025013 (2010)
[57]. E. de la Luna et al., 23rd IAEA Fusion Energy Conference, Daejon (2010)

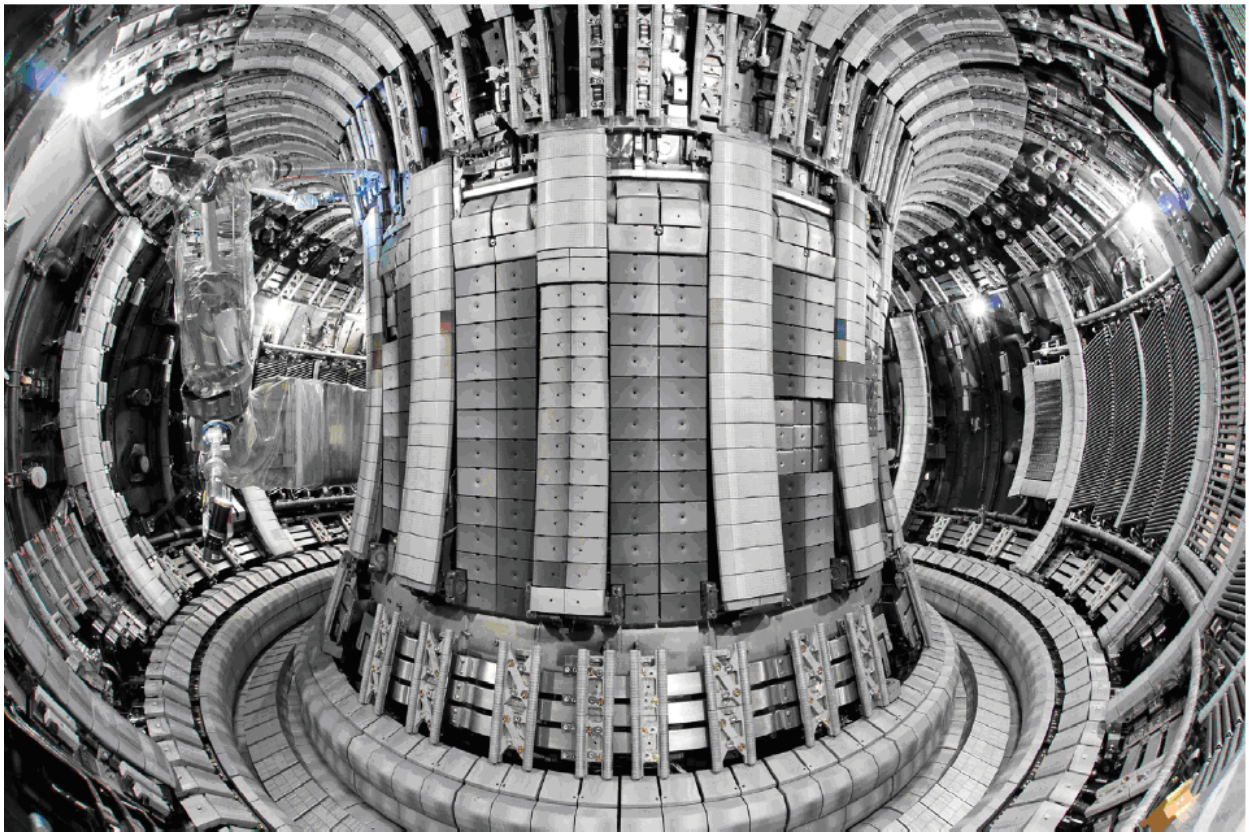

Figure 1: The new JET ITER-like wall. The main wall tiles are either bulk-Be or Be coated Inconel with W-coated tiles used for the NBI shine through areas and restraint rings. The divertor is composed of bulk W tiles for the horizontal target and W-coated CFC tiles for the rest.

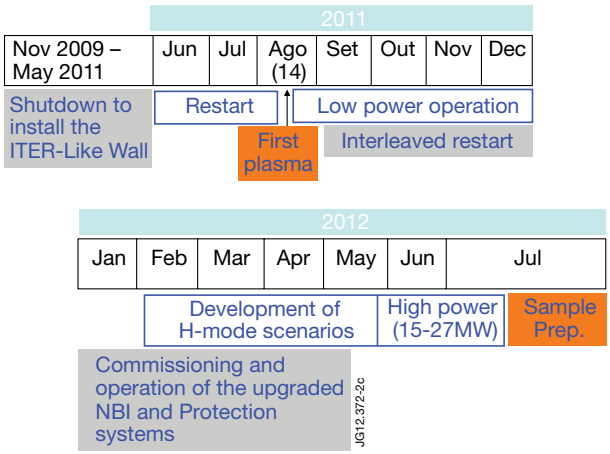

Figure 2: Time line of JET operation in 2011 and 2012.

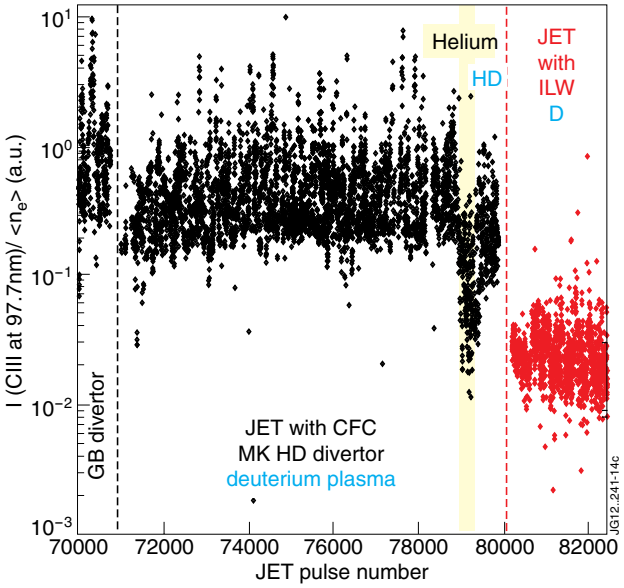

Figure 3: Evolution of the normalised carbon edge emission showing a clear decrease (~20×) after the installation of the ILW.

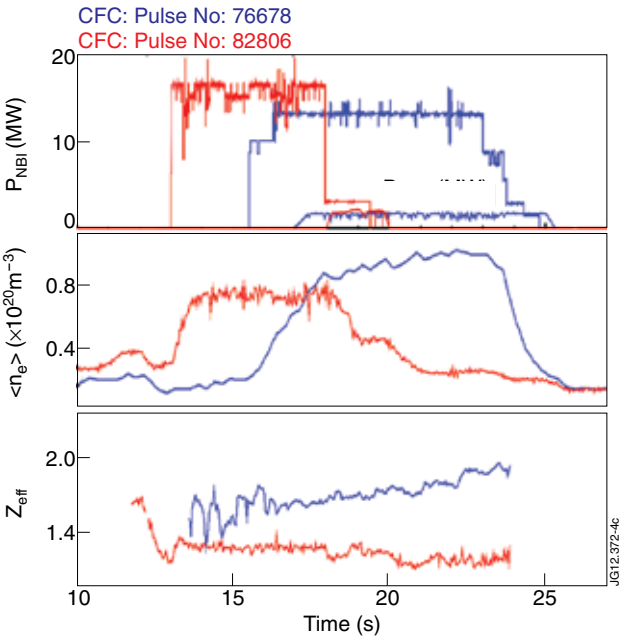

Figure 4: Traces of Zeff between two similar discharges in JET-C and JET-ILW.

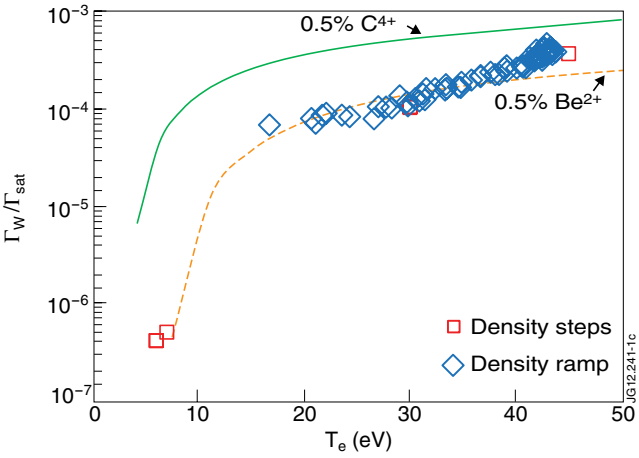

Figure 5: Effective W erosion yields measured in low power L-mode. Values follow very close the predicted erosion rates for a 0.5% (experimental) abundance of Be2+. For comparison, the expected erosion yield for the impact of C4+ ions is shown as green line.

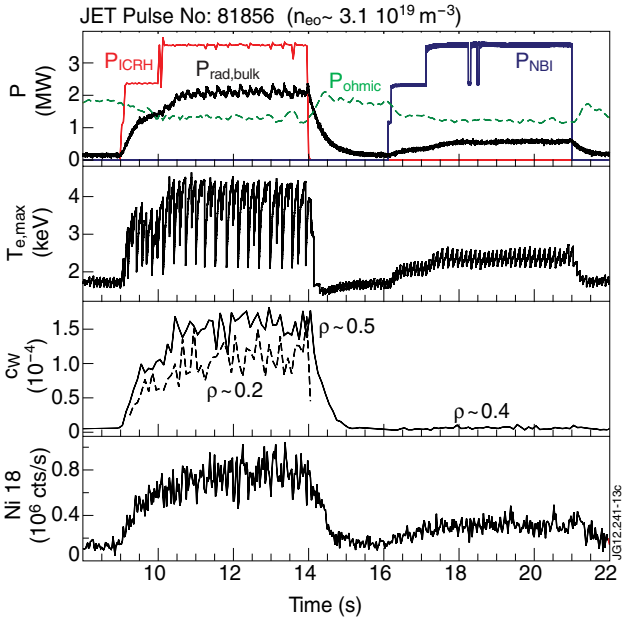

Figure 6: The effect of ICRF and neutral beam heating on plasma radiation, central elctron temperature, W concentration and Ni emission in an L-mode plasma at constant density.

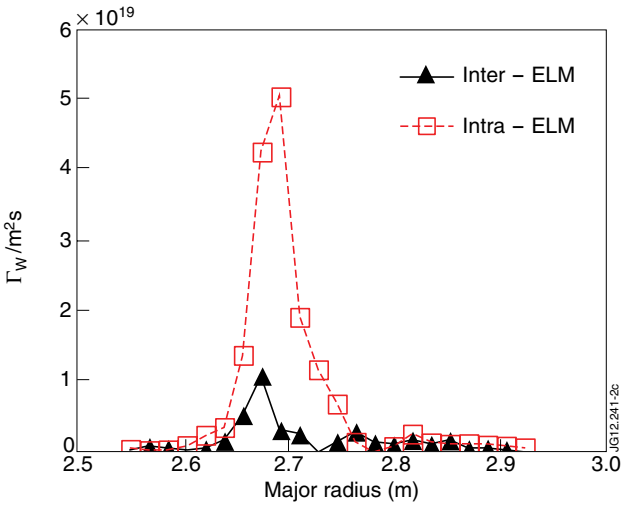

Figure 7: Comparison of the tungsten influx (time averaged) between and during ELMs . The graph shows clearly that intra-ELM W-sputtering is largely dominant (13 MW NBI, 7.5×10^19 m^-3 line averaged n_e, 10Hz fELM).

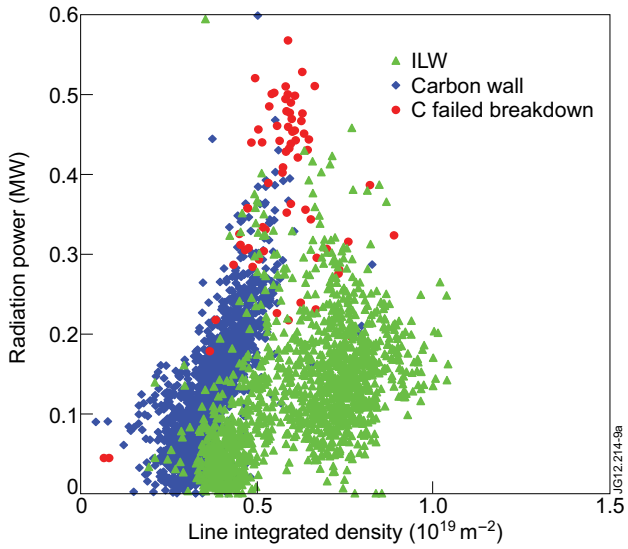

Figure 8: Radiation power versus line-integrated density at the end of the burn-through phase in JET.

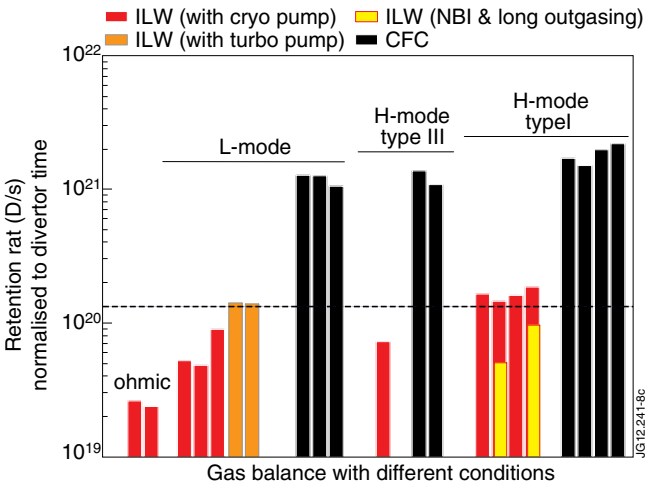

Figure 9: Retention rates for ILW and C wall in different types of plasma.

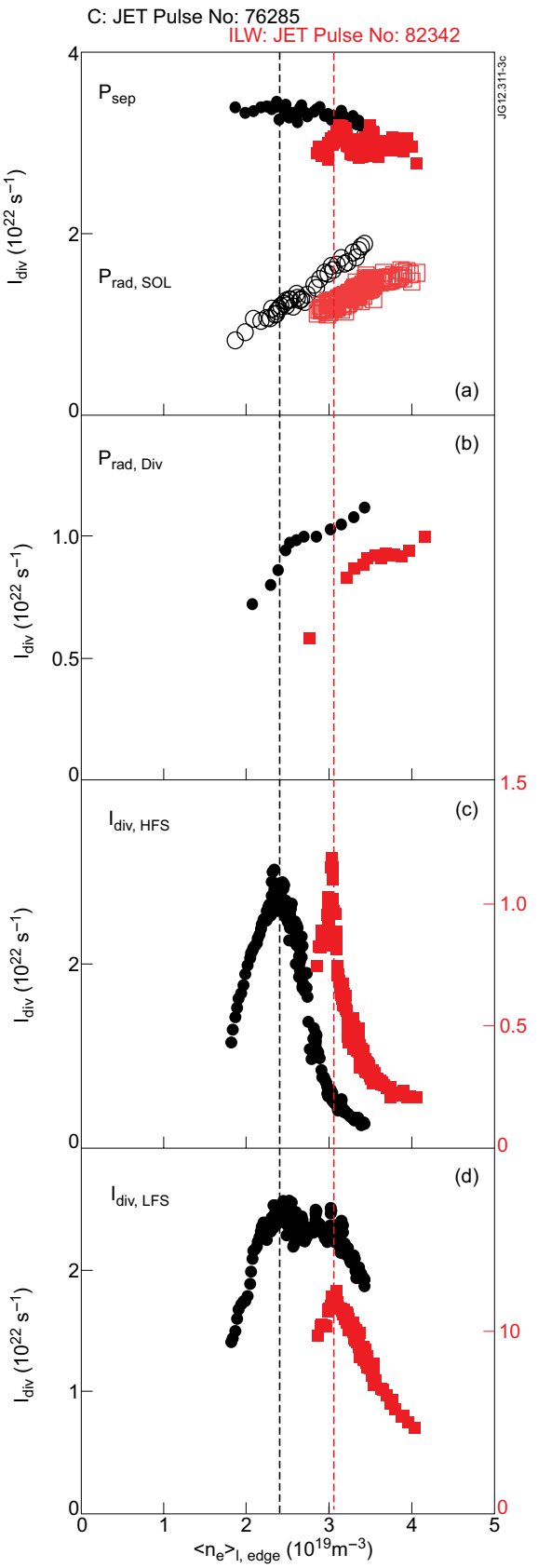

Figure 10: Total power across the separatrix and radiated power in the SOL (a), total radiated power in divertor (b), and total ion currents to the HFS (c) and LFS plates (d) as function of lineaveraged edge density.

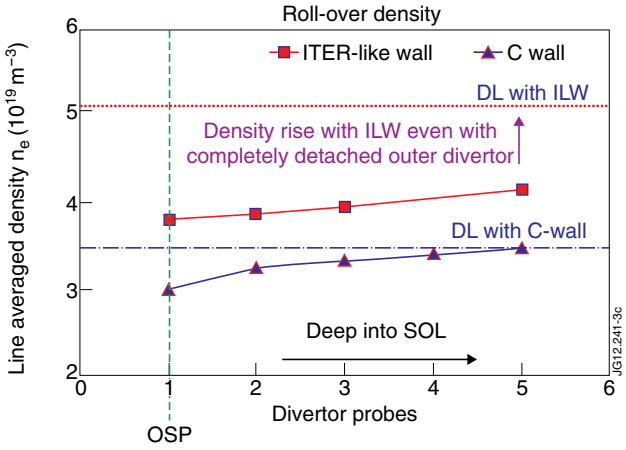

Figure 11: Roll-Over and density limits for operation with detached divertor for C machine and ILW. The density is measured by a Langmuir probe array along the divertor. In the ILW the detachment occurs at much lower density, below the L-H transition limit, giving larger margin for stable detachment operation.

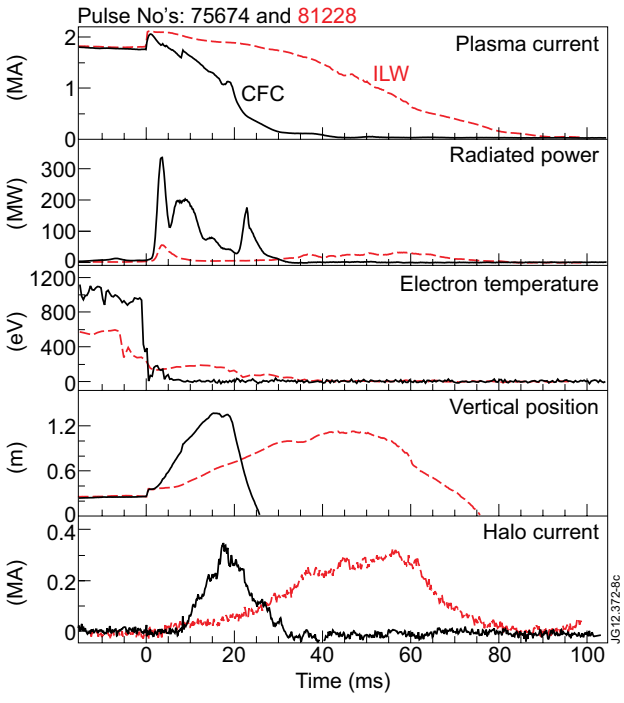

Figure 12: Comparison of disruption characteristics between JET-C (black) and JET-ILW (red).

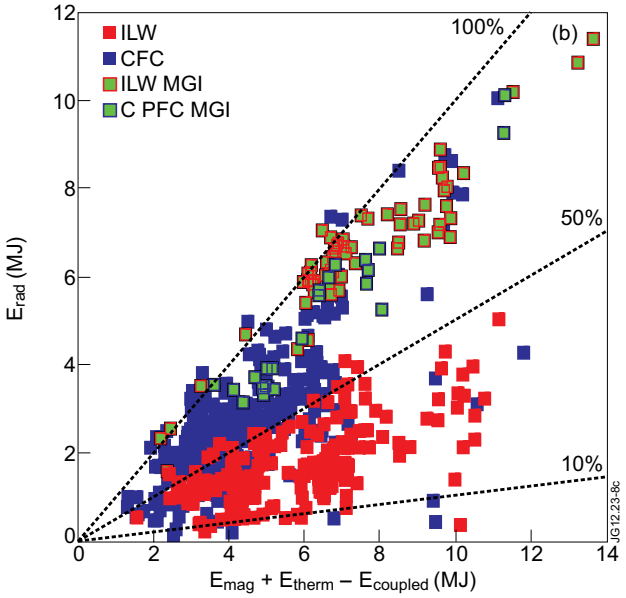

Figure 13: Radiated energy as function of the energy available in the plasma. The green dots represent disruptions in JET-ILW with the use of MGI.

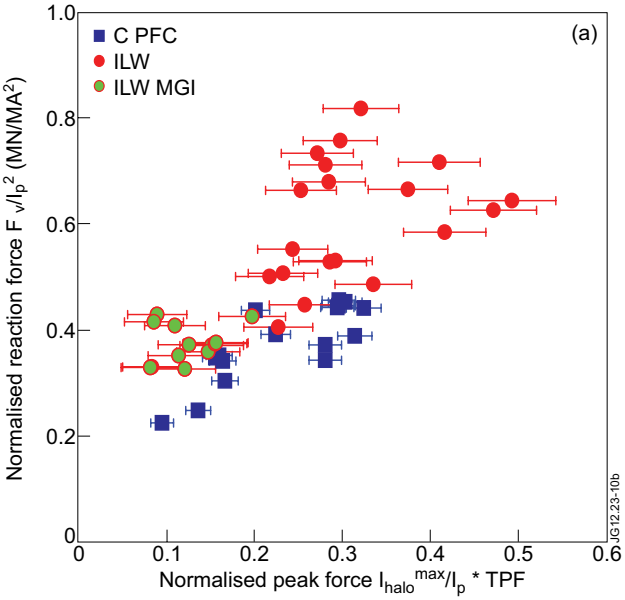

Figure 14: The equivalent static force required for the measured vessel excursion normalised to the plasma current squared versus the normalised halo current force for a set of high triangularity JET-C and JET-ILW disruptions. The green dots represent disruptions in JET-ILW with the use of MGI.

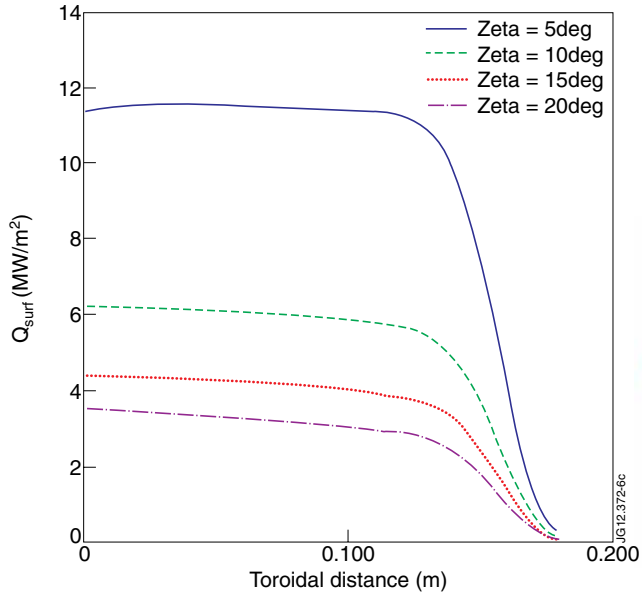

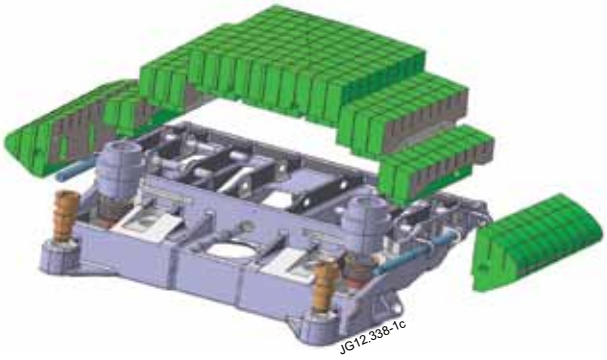

Figure 15: On the left is shown the variation of the power load on the surface of the divertor tile when the q95-profile varies (scanning the zeta angle). On the right is shown a Be tile composed of separated blocks which are designed to take into account minimization of image currents and power handling at the expected range of field line angles for each exposed surface.

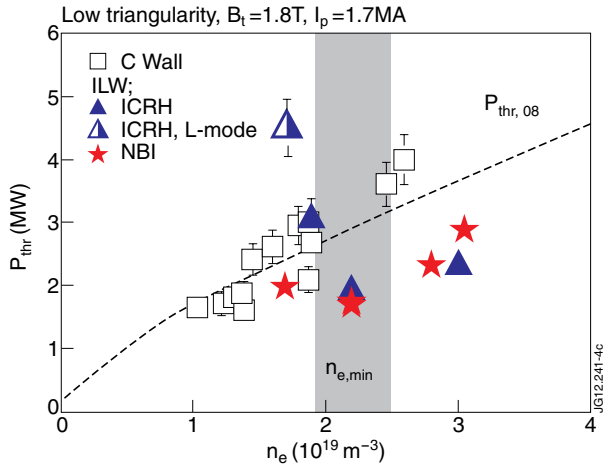

Figure 16: H-mode power threshold comparison between JET-C and JET-ILW.

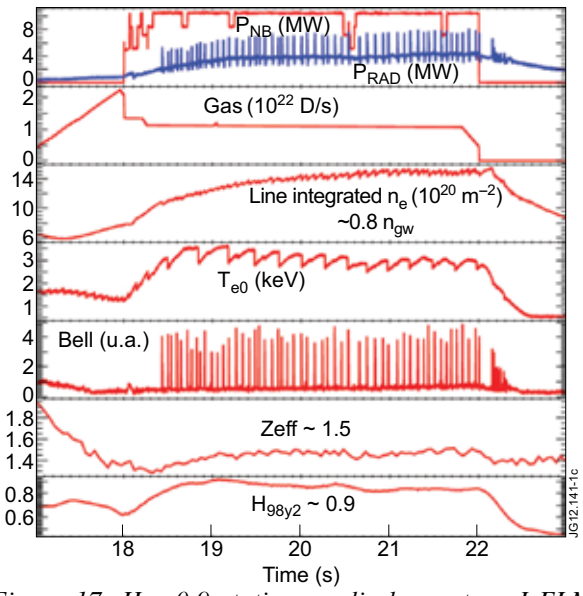

Figure 17: H_{98}~0.9 stationary discharge type I ELM baseline scenario with the JET ILW (NBI: 11 MW).

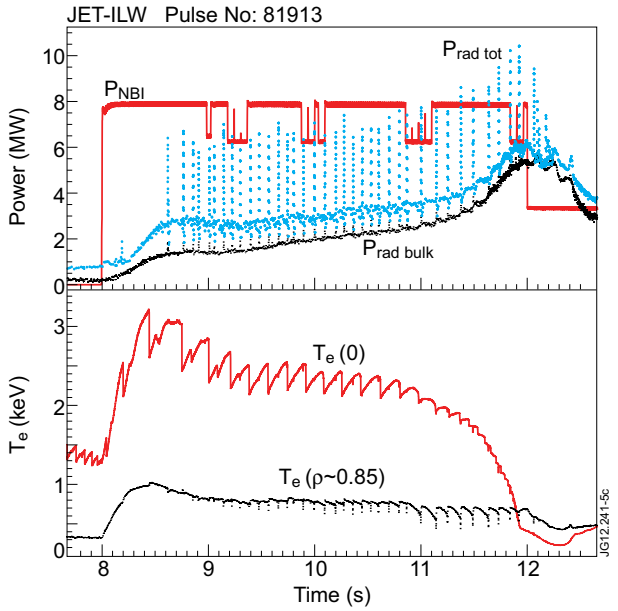

Figure 18: Extreme example of W peaking and accumulation. A rise in central radiated power leads to a collapse of the central temperature.

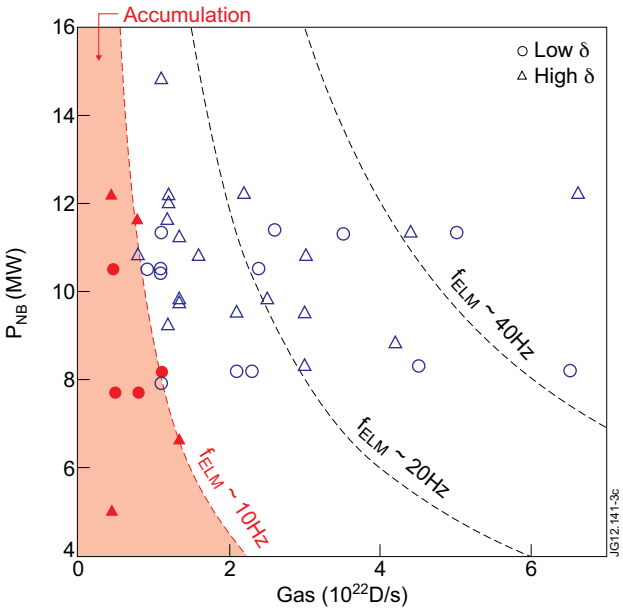

Figure 19: ILW operating space in the PNB versus deuterium gas puffing rate at 2.0MA/2.1-2.2T.

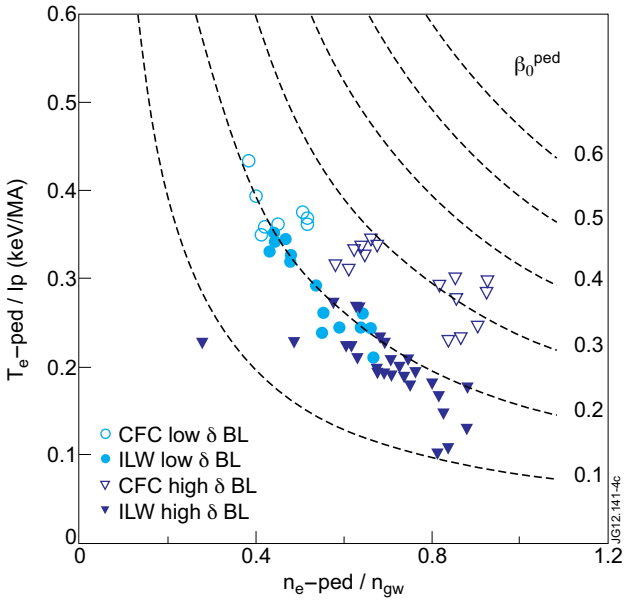

Figure 20: {T_e-ped/I_p, n_e-ped/ngw} diagram comparing C wall and ILW at 2.5MA/2.7T. (BL – baseline).

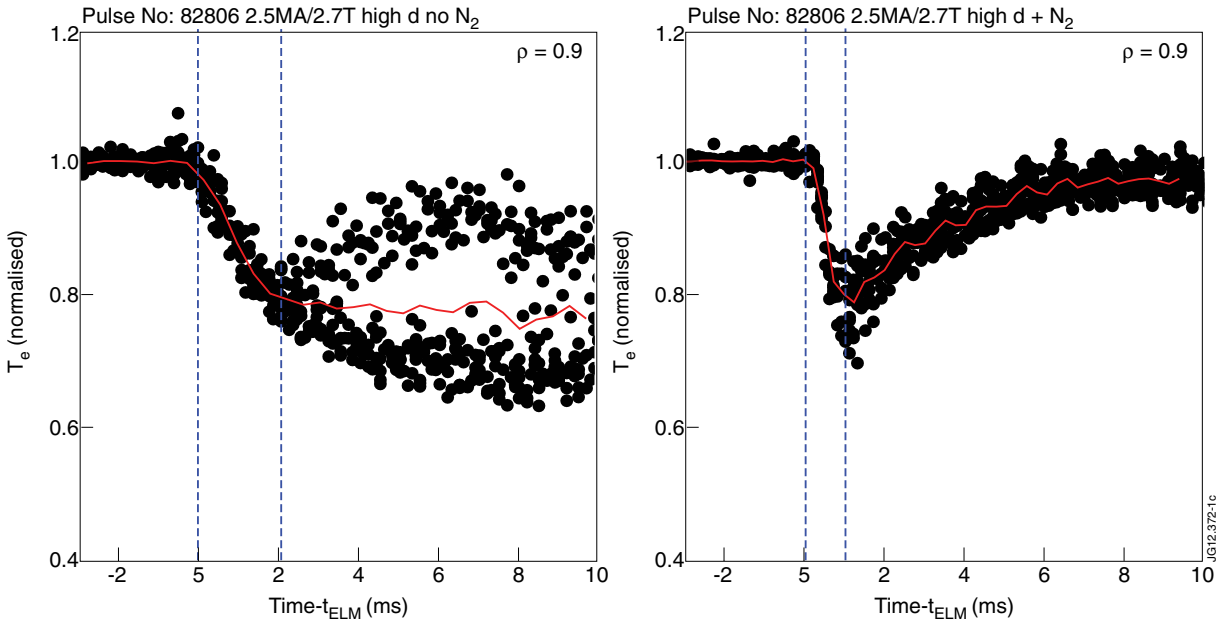

Figure 21: Edge electron temperature measured by ECE for type I ELMs with JET-ILW: left - for a deuterium fuelled pulse showing a slow temperature crash (T_e,ped = 500eV) and a bifurcated recovery; right - a similar nitrogen seeded pulse where the crash is much faster (T_e,ped = 770eV).

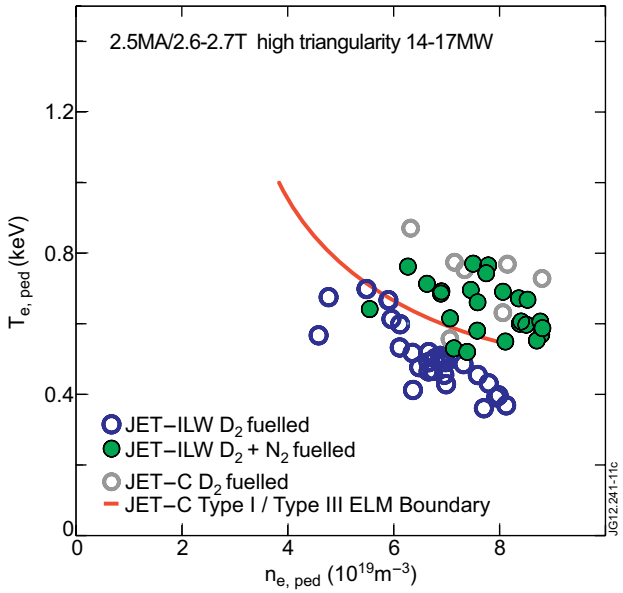

Figure 22: Pedestal n_e, T_e diagram for high triangularity pulses with similar input power (14-17MW). The data shows that JET-C pedestal conditions can be recovered in the JET-ILW via N_2 seeding.

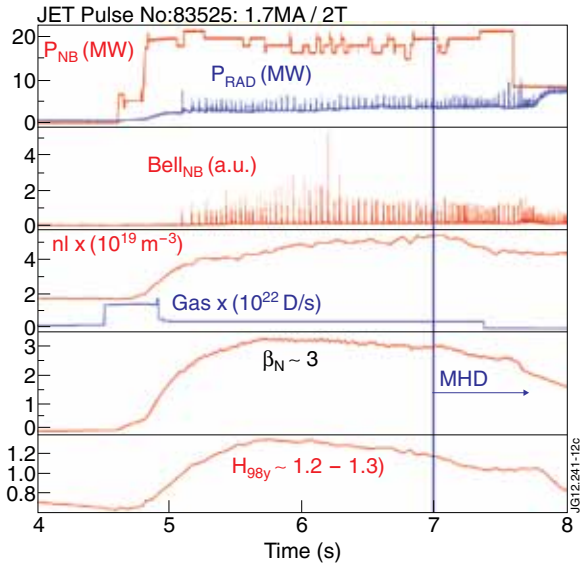

Figure 23: Example for a "hybrid" plasma (1.5MA / 2.0T) [46] in JET-ILW at $H_{98y2} > 1$ at low total radiated power and Z_{eff}.

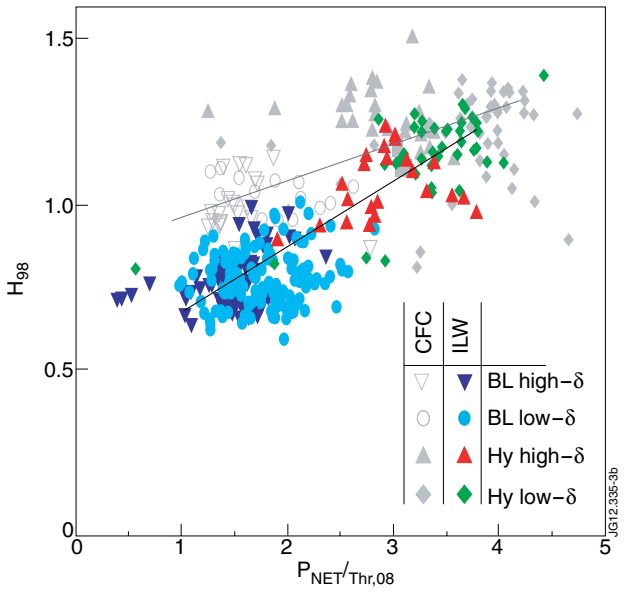

Figure 24: H_{98} versus the ratio of $P_{net}/P_{thr,08}$ for JET-C (gray) and JET-ILW Hybrid and baseline ELMy H-mode plasmas overlaid (right). To note that the actual Pthr as measured in the ILW experiments is lower than Pthr,08. The two lines are linear fits to the data.

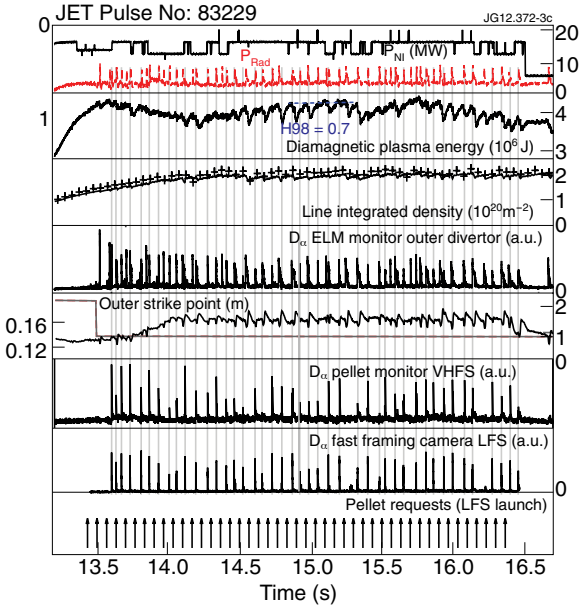

Figure 25: Sustainment of ELM activity preventing impurity accumulation by (fuelling size) pellet pacing at 15Hz rate in the ITER baseline scenario (2.5MA high shaping). Despite the strong extra fuelling introduced by the pellets (estimated about 2.6 ×10^{22} D/s) only a mild density increase and no reduction of confinement is observed.

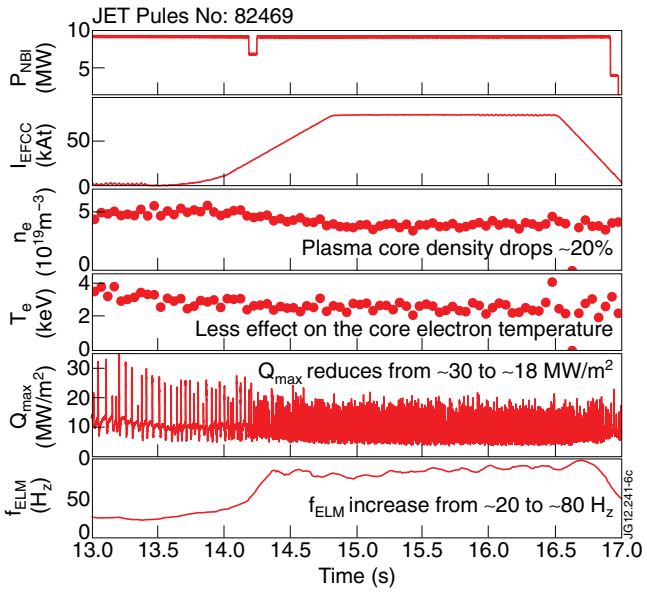

Figure 26: An example of ELM mitigation with the n = 2 field in a low collisionality type-I ELM H-mode plasma.

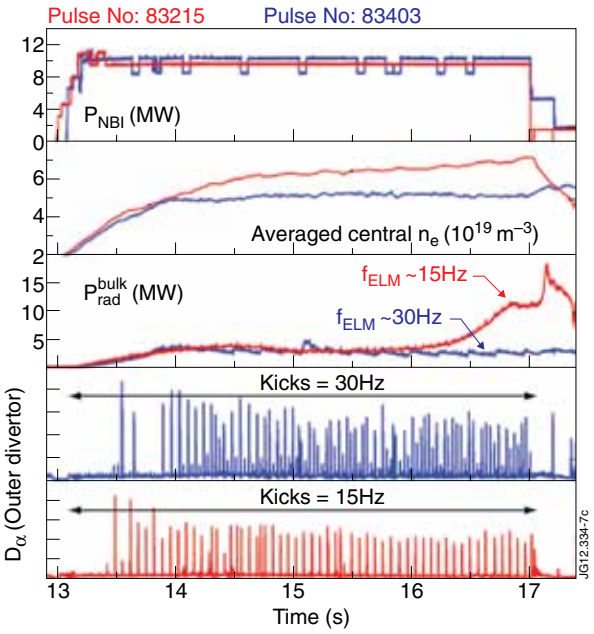

Figure 27: ELM pacing experiments using vertical kicks in gas fuelled H-modes plasmas in JET with the Be/W wall (I_p = 2MA, B_T = 2.2T, q_{95} = 3.6, H_{98}~0.9, d_{av}~0.3). Core W accumulation is seen with f_{ELM} = 15Hz but not with f_{ELM} =30Hz.

Appendix: List of JET EFDA Contributors

I. Abel[1], V. Afanesyev[2], M. Aftanas[3], G. Agarici[4], K.M. Aggarwal[5], L. Aho-Mantila[6], E. Ahonen[7], M. Aints[8], M. Airila[6], R. Akers[9], Th. Alarcon[4], R. Albanese[10], A. Alexeev[11,12], A. Alfier[13], P. Allan[9], S. Almaviva[14], A. Alonso[15], B. Alper[9], H. Altmann[9], D. Alves[16], G. Ambrosino[10], V. Amosov[12], F. Andersson[17], E. Andersson Sundén[18], V. Andreev[11], Y. Andrew[9], M. Angelone[19], M. Anghel[20], A. Anghel[21], C. Angioni[22], G. Apruzzese[19], N. Arcis[9], P. Arena[23], A. Argouarch[4], M. Ariola[10], A. Armitano[4], R. Armstrong[24], G. Arnoux[9], S. Arshad[25], G. Artaserse[10], J.F. Artaud[4], A. Ash[9], E. Asp[18], O. Asunta[7], C.V. Atanasiu[21], G. Atkins[9], L. Avotina[26], M.D. Axton[9], C. Ayres[9], A. Baciero[15], V. Bailescu[27], B. Baiocchi[28], R.A. Baker[9], I. Balboa[9], M. Balden[22], C. Balorin[4], N. Balshaw[9], J.W. Banks[9], Y.F. Baranov[9], D. Barbier[4], I.L. Barlow[9], M.A. Barnard[9], R. Barnsley[5], L. Barrena[15], L. Barrera[15], M. Baruzzo[13], V. Basiuk[4], G. Bateman[29], P. Batistoni[19], N. Baumgarten[30], L. Baylor[31], B. Bazylev[32], P.S. Beaumont[9], K. Beausang[24], M. Bécoulet[4], N. Bekris[33,32], M. Beldishevski[9], A.C. Bell[9], F. Belli[19], M. Bellinger[9], T. Bellizio[10], P.S.A. Belo[16], É. Belonohy[22], P.E. Bennett[9], N.A. Benterman[9], G. Berger-By[4], H. Bergsåker[34], H. Berk[35], J. Bernardo[16], M. Bernert[22], B. Bertrand[4], M.N.A. Beurskens[9], B. Bieg[36], B. Bienkowska[36], T.M. Biewer[31], M. Bigi[13], P. Bílková[3], W. Bin[28], J. Bird[9], J. Bizarro[16], C. Björkas[37], T.R. Blackman[9], P. Blanchard[38], E. Blanco[15], J. Blum[39], V. Bobkov[22], A. Boboc[9], D. Boilson[24], I. Bolshakova[40], T. Bolzonella[13], L. Boncagni[19], G. Bonheure[41], X. Bonnin[4], D. Borba[33,16], A. Borthwick[9], A. Botrugno[19], C. Boulbe[39], F. Bouquey[4], C. Bourdelle[4], K.v. Bovert[30], M. Bowden[9], T. Boyce[9], H.J. Boyer[9], A. Bozhenkov[30], R.J. Brade[9], J.M.A. Bradshaw[9], J. Braet[42], V. Braic[43], G.C. Braithwaite[9], C. Brault[4], B. Breizman[35], S. Bremond[4], P.D. Brennan[9], A. Brett[9], J. Breue[44], S. Brezinsek[30], M.D.J. Bright[9], F. Briscoe[9], M. Brix[9], M. Brombin[13], B.C. Brown[9], D.P.D. Brown[9], J. Brzozowski[34], J. Bucalossi[4], M.A. Buckley[9], T. Budd[9], R.V. Budny[45], P. Bunting[9], P. Buratti[19], G. Burcea[27], A. Burckhart[22], P.R. Butcher[9], R.J. Buttery[46], P. Cahyna[3], G. Calabrò[19], C.P. Callaghan[9], J.P. Caminade[4], P.G. Camp[9], D.C. Campling[9], R. Caniello[28], J. Canik[31], B. Cannas[47], A.J. Capel[9], G. Carannante[10], P.J. Card[9], A. Cardinali[19], T. Carlstrom[46], P. Carman[9], D. Carralero[15], L. Carraro[13], T. Carter[48], B.B. Carvalho[16], I. Carvalho[16], P. Carvalho[16], A. Casati[4], C. Castaldo[19], J. Caughman[31], R. Cavazzana[13], M. Cavinato[13], M. Cecconello[18], E. Cecil[45], F.E. Cecil[49], A. Cenedese[13], C. Centioli[19], R. Cesario[19], C.D. Challis[9], M. Chandler[9], C. Chang[50], A. Chankin[22], I.T. Chapman[9], B. Chektybayev[51], M. Chernyshova[36], D.J. Child[9], P. Chiru[21], G. Chitarin[13], I. Chugonov[2], I. Chugunov[2], D. Ciric[9], F. Clairet[4], R.H. Clarke[9], R. Clay[9], M. Clever[30], J.P. Coad[9,6], P.A. Coates[9], V. Cocilovo[19], S. Coda[38], R. Coelho[16], J. Coenen[30], I. Coffey[5], L. Colas[4], M. Cole[31], S. Collins[9], S. Combs[31], J. Compan[44], J.E. Conboy[9], S. Conroy[18], N. Cook[9], S.P. Cook[9], D. Coombs[9], S.R. Cooper[9], Y. Corre[4], G. Corrigan[9], S. Cortes[16], D. Coster[22], G.F. Counsell[9], X. Courtois[4], M. Cox[9], T. Craciunescu[21], S. Cramp[9], F. Crisanti[19], G. Croci[28], O. Croft[9], K. Crombe[52], K. Crombé[53], B.J. Crowley[9], N. Cruz[16], G. Cseh[54], L. Cupido[16], M. Curuia[20], R.A. Cusack[9], A. Czarnecka[36], T. Czarski[36], S. Dalley[9], E.T. Daly[9], A. Dalziel[9], R. Daniel[55], D. Darrow[45], O. David[56], N. Davies[9], W. Davies[45], J.J. Davis[9], I.E. Day[9], C. Day[32], R. De Angelis[19], G. de Arcas[57], M.R. de Baar[58], E. de la Cal[15], E. de la Luna[15,33], J.L. de Pablos[15], G. De Tommasi[10], P.C. de Vries[58], R.

De-Angelis[19], F. Degli Agostini[13], E. Delabie[58], D. del-Castillo-Negrete[31], L. Delpech[4], G. Denisov[59], A.J. Denyer[9], R.F. Denyer[9], S. Devaux[22], P. Devynck[4], L. Di Matteo[19], L. Di Pace[19], P.J. Dirken[9], T. Dittmar[60], A. Dnestrovskiy[11], D. Dodt[22], R. Doerner[60], S. Doldatov[52], K. Dominiczak[44], P. Dooley[33,19], S.E. Dorling[9], D. Douai[4], A.P. Down[9], P.T. Doyle[9], J.R. Drake[34], T. Dreischuh[61], V. Drozdov[9], P. Dumortier[53], D. Dunai[54], I. Duran[3], F. Durodié[53], P. Dutta[55], R. Dux[22], K. Dylst[42], R. Eaton[9], T. Edlington[9], A.M. Edwards[9], D.T. Edwards[9], P.K. Edwards[9], Th. Eich[22], A. Ekedahl[4], T. Elevant[34], B. Ellingboe[24], C.G. Elsmore[9], B. Emmoth[62], G. Erdei[63], G. Ericsson[18], L.G. Eriksson[64], A. Eriksson[17], B. Esposito[19], H.G. Esser[30], T. Estrada[15], E.A. Evangelidis[65], G.E. Evans[9], G.D. Ewart[9], D.T. Ewers[9], G. Falchetto[4], D. Falie[21], J.G.A. Fanthome[9], J.W. Farthing[9], A. Fasoli[38], B. Faugeras[39], N. Fedorczak[4], R.C. Felton[9], C. Fenzi[4], A. Fernades[16], H. Fernandes[16], J.A. Ferreira[15], J. Ferreira[16], J. Ferron[46], J.A. Fessey[9], L. Figini[28], J. Figueiredo[33], A. Figueiredo[16], J. Figueiredo[16], P. Finburg[9], K.H. Finken[30], U. Fischer[32], N. Fitzgerald[24], J. Flanagan[9], C. Fleming[9], A.D. Forbes[9], O. Ford[1], A. Formisano[10], D. Fraboulet[4], R.J. Francis[9], L. Frassinetti[34], R. Fresa[10], J.P. Friconneau[56], D. Frigione[19], K. Fullard[9], W. Fundamenski[9], M. Furno Palumbo[10], K. Gál[54], X. Gao[66], S. Garavaglia[28], X. Garbet[4], J. Garcia[4], M. Garcia Munoz[22], W. Gardner[31], P. Garibaldi[4], D. Garnier[4], L. Garzotti[9], M. Gatu Johnson[18], P. Gaudio[14], E. Gauthier[4], J.W. Gaze[9], D.F. Gear[9], J. Gedney[9], S.J. Gee[9], M. Gelfusa[14], E. Genangeli[33,19], S. Gerasimov[9], A. Geraud[4], T. Gerbaud[4,58], M. Gherendi[21], N. Ghirelli[4], J.C. Giacalone[4], L. Giacomelli[41], C.S. Gibson[9], C. Gil[4], S.J. Gilligan[9], C.G. Gimblett[9], D. Gin[2], E. Giovannozzi[19], C. Giroud[9], G. Giruzzi[4], J. Godwin[9], J.K. Goff[9], P. Gohil[46], A. Gójska[36], V. Goloborod'ko[67], B. Gonçalves[16], M. Goniche[4], S. Gonzales[15], S.M. González de Vicente[42], A. Goodyear[9], N. Gorelenkov[45], G. Gorini[41], R. Goulding[31], B. Graham[9], D. Graham[9], M.E. Graham[9], J. Graves[38], N.R. Green[9], H. Greuner[22], E. Grigore[21], F.S. Griph[9], C. Grisolia[4], G. Gros[4], M. Groth[7], S. Grünhagen[9], M.P. Gryaznevich[9], R. Guirlet[4], J. Gunn[4], A. Gupta[30], P. Guzdar[68], L.J. Hackett[9], S. Hacquin[4], B. Haist[9], A. Hakola[6], M. Halitovs[26], S.J. Hall[9], S.P. Hallworth Cook[9], D.T. Hamilton[9], H. Han[69], R.C. Handley[9], S. Harding[9], J.D.W. Harling[9], D. Harting[30], M.J. Harvey[9], T.D.V. Haupt[9], N.C. Hawkes[9], R. Hawryluk[45], J.H. Hay[9], N. Hayashi[50], P.W. Haydon[9], I.R. Hayward[9], S. Hazel[9], P.J.L. Heesterman[9], W. Heidbrink[45], K. Heinola[37], C. Hellesen[18], T. Hellsten[34], O.N. Hemming[9], T.C. Hender[9], M. Henderson[70], V. Hennion[4], C. Hidalgo[15], S. Higashijima[50], J.W. Hill[9], M. Hill[9], K. Hill[45], J. Hillairet[4], D. Hillis[31], T. Hirai[44], M. Hitchin[9], J. Hobirk[22], C. Hogan[31], C.H.A. Hogben[9], G.M.D. Hogeweij[58], I.C. Hollingham[9], R. Holyaka[40], D.A. Homfray[9], G. Honeyands[9], S.H. Hong[4], J.H. Hong[71], J. Horácek[3], B.A. Horn[9], A.R. Horton[9], L.D. Horton[33,64], S.P. Hotchin[9], M.R. Hough[9], W. Houlberg[31], D.F. Howell[9], A. Huber[30], T.M. Huddleston[9], Z. Hudson[9], M. Hughes[9], M. Hühnerbein[44], C.C. Hume[9], A.J. Hunt[9], C.L. Hunter[9], T.S. Hutchinson[9], S. Huygen[53], G. Huysmans[4], S. Ide[50], C. Illescas[15], F. Imbeaux[4], D. Ivanova[34], I. Ivanova-Stanik[36], E. Ivings[9], S. Jachmich[53], G. Jackson[46], P. Jacquet[9], K. Jakubowska[36], P.V. James[9], F. Janky[3], A. Järvinen[7], S. Jednorog[36], I. Jenkins[9], M.A.C. Jennison[9], C. Jeskins[9], O. Jin Kwon[72], E. Joffrin[4,33], M.F. Johnson[9], R. Johnson[9], T. Johnson[34], D. Jolovic[30], V. Jonauskas[73], E.M. Jones[9], G. Jones[9], H.D. Jones[9], T.T.C. Jones[9], M. Jouvet[4], C. Jupén[74], I. Kachtchouk[12], J. Kaczmarczyk[36], A. Kallenbach[22], J. Källne[75], D. Kalupin[30],

S. Kálvin[54], G. Kamelander[76], R. Kamendje[77], K. Kamiya[50], A. Kappatou[78], W. Kasparek[79], G. Kasprowicz[36], I. Katramados[9], G. Kaveney[9], A.S. Kaye[9], M.J. Kear[9], D.L. Keeling[9], D. Kelliher[24], M. Kempenaars[9], P. Khilar[9], E. Khilkevich[2], N.G. Kidd[9], M. Kiisk[8], K.M. Kim[69], H. Kim[69], R.F. King[9], D.J. Kinna[9], V. Kiptily[9], G. Kirnev[11], N. Kirneva[11], K. Kirov[9], A. Kirschner[30], R. Kisielius[73], D. Kislov[11], G. Kiss[30], G. Kizane[26], A. Klein[80], C. Klepper[31], N. Klimov[12], A. Klix[32], M. Knaup[30], K. Kneuper[9], H. Kneupner[30], P.J. Knight[9], S.J. Knipe[9], M. Kocan[4], R. Koch[53], F. Köchl[76], G. Kocsis[54], S. Koivuranta[6], T. Koppitz[44], A. Korotkov[9], T. Koskela[7], H.R. Koslowski[30], V. Kotov[30], M.D. Kovari[9], G. Kramer[45], A. Krasilnikov[12], V. Krasilnikov[12], S. Kraus[30], A. Kreter[30], K. Krieger[22], A. Kritz[29], Y. Krivchenkov[9], U. Kruezi[30], S. Krylov[11], I. Ksiazek[36], S. Kuhn[67], W. Kühnlein[44], A. Kukushkin[11], A. Kundu[55], T. Kurki-Suonio[7], A. Kurowski[36], B. Kuteev[11], A. Kuyanov[11], V. Kyrytsya[53], R. La Haye[46], M. Laan[8], C. Labate[10], A. Lachichi[9], L. Laguardia[28], N. Lam[9], P. Lang[22], M.T. Large[9], A. Lasa[37], I. Lassiwe[30], J.R. Last[9], K.D. Lawson[9], M. Laxåback[34], R.A. Layne[9], F. Le Guern[4], B. LeBlanc[45], S. Lee[81], J. Lee[69], H.J. Leggate[24], M. Lehnen[30], M. Leigheb[19], I. Lengar[82], M. Lennholm[33,64], E. Lerche[53], C.N. Lescure[9], Y. Li[80], A. Li Puma[4], Y. Liang[30], J. Likonen[6], Y. Lin[80], V. Lindholm[7], J. Linke[44], S.A. Linstead[9], B. Lipshultz[80], X. Litaudon[4], A.G. Litvak[59], Y. Liu[9,66], T. Loarer[4], A. Loarte[70], R.C. Lobel[9], P.J. Lomas[9], F.D. Long[9], J. Lönnroth[7], D.J. Looker[9], J. Lopez[15], Ph. Lotte[4], F. Louche[53], M.J. Loughlin[9], A.B. Loving[9], C. Lowry[33,64], T. Luce[46], R.M.A. Lucock[9], A. Lukanitsa[83], A. Lukin[84], A.M. Lungu[21], C.P. Lungu[21], A. Lyssoivan[53], P. Macheta[9], A.S. Mackenzie[9], M. Macrae[9], G. Maddaluno[19], G.P. Maddison[9], J. Madsen[85], B. Magesh[55], P. Maget[4], C.F. Maggi[22], H. Maier[22], J. Mailloux[9], T. Makkonen[7], M. Makowski[46], A. Malaquias[33,16], C.J. Manning[9], M. Mansfield[24], M.E. Manso[16], P. Mantica[28], N. Marcenko[12], M.A. Marchitti[10], M. Mardenfeld[45], J.L. Marechal[4], M. Marinelli[14], M. Marinucci[19], D. Marocco[19], C.A. Marren[9], S. Marsen[86], D. Martin[9], D.L. Martin[9], G. Martin[4], Y. Martin[38], J.R. Martín-Solís[87], K. Masaki[50], A. Masiello[13], C. Maszl[67], S. Matejcik[88], A. Matilal[9], M. Mattei[10], G.F. Matthews[9], S. Mattoo[55], D. Matveev[52], F. Maviglia[10], C.R. May[9], M. Mayer[22], M.L. Mayoral[9], D. Mazon[4], C. Mazzotta[19], E. Mazzucato[45], P. McCarthy[24], K.G. McClements[9], K. McCormick[22], P.A. McCullen[9], D. McCune[45], D.C. McDonald[9], R. Mcgregor[9], J.P. Mckivitt[9], A. Meakins[9], F. Medina[15], A.G. Meigs[9], M. Menard[46], L. Meneses[16], S. Menmuir[89], I.R. Merrigan[9], Ph. Mertens[30], A. Messiaen[53], B. Mészáros[54], H. Meyer[9], G. Miano[10], R. Michling[32], M. Miele[10], J. Miettunen[7], P. Migliucci[14], A.G. Miller[9], S.F. Mills[9], J.J. Milnes[9], K. Min Kim[69], T. Mindham[9], E. Miorin[28], F. Mirizzi[19], E. Mirones[15], M. Mironov[2], R. Mitteau[4], J. Mlynár[3], P. Mollard[4], I. Monakhov[9], P. Monier-Garbet[4], R. Mooney[9], D. Moreau[4], Ph. Moreau[4], L. Moreira[9], A. Morgan[9], P.D. Morgan[9], C. Morlock[90,30], A.W. Morris[9], G.L. Mort[9], M. Murakami[31], A. Murari[33,13], I. Mustata[21], F. Nabais[16], T. Nakano[50], E. Nardon[4], G. Nash[9], V. Naulin[85], M.F.F. Nave[16], R. Nazikian[45], I. Nedzelski[16], C.R. Negus[9], J.D. Neilson[9], G. Nemtsev[12], A. Neto[16], R. Neu[22], O. Neubauer[30], G.J. Newbert[9], M. Newman[9], K.J. Nicholls[9], A. Nicolai[30], L. Nicolas[4], P. Nieckchen[90,22], A.H. Nielsen[85], S.K. Nielsen[85], P. Nielsen[13], G. Nielson[45], J. Nieto[57], M.P.S. Nightingale[9], D. Nishijima[55], C. Noble[9], M. Nocente[41], H. Nordman[17], M. Norman[9], S. Nowak[28], I. Nunes[16], M. Oberkofler[22], M. Odstrcil[3], T. O'Gorman[24], T. Ohsako[50], M. Okabayashi[45],

S. Olariu[91], A. Oleynikov[12], M. O'Mullane[92], J. Ongena[53], F. Orsitto[19], O.I. Oswuigwe[9], M. Ottaviani[4], N. Oyama[50], D. Pacella[19], K. Paget[9], E. Pajuste[26], S. Palazzo[23], J. Palénic[88], J. Pamela[4], S. Pamela[4], L. Pangione[9], A. Panin[30], S. Panja[55], A. Pankin[29], A. Pantea[21], V. Parail[9], P. Paris[8], Th. Parisot[4], M. Park[81], A. Parkin[9], A. Parsloe[9], B.T. Parsons[9], R. Pasqualotto[13], P. Pastor[4], R. Paterson[9], M.K. Paul[30], D. Peach[9], R.J.H. Pearce[9], B.J. Pearson[9], I.J. Pearson[9], L.C. Pedrick[9], M.A. Pedrosa[15], B. Pegourie[4], R. Pereira[16], P. Pereslavtsev[32], A. Perevezentsev[9], Ch. Perez von Thun[33,22], V. Pericoli-Ridolfini[90,19], A. Perona[93], Y. Perrot[56], S. Peruzzo[13], S. Peschanyy[32], G. Petravich[54], L. Petrizzi[19], V. Petrov[12], V. Petrzilka[3], V. Philipps[30], F. Piccolo[9], A. Pietropaolo[28], M. Pillon[19], S.D. Pinches[9], T. Pinna[19], G. Pintsuk[44], P. Piovesan[13], A. Pironti[10], F. Pisano[47], R. Pitts[70], B. Plaum[79], V. Plyusnin[16], M. Polasik[36], F.M. Poli[94], N. Pomaro[13], O. Pompilian[21], L. Poncet[4], P.J. Pool[9], S. Popovichev[9], F. Porcelli[93], M.T. Porfiri[19], C. Portafaix[4], A. Pospieszczyk[30], G. Possnert[75], K. Pozniak[36], S. Pradhan[55], R. Pragash[55], V. Prajapati [55], G. Prestopino[14], P. Prior[9], R. Prokopowicz[36], M.E. Puiatti[13], K. Purahoo[9], V. Pustovitov[11], Th. Pütterich[22], D. Püttmann-Kneupner[30], A. Quercia[10], E. Rachlew[89], R. Rademaker[33], T. Rafiq[29], M.S.J. Rainford[9], G. Ramogida[19], J. Rapp[30], J.J. Rasmussen[85], K. Rathod[55], G. Rattá[15], G. Ravera[19], D. Refy[54,63], R. Reichle[4], M. Reinelt[22], D. Reiser[30], R. Reiss[4], D. Reiter[30], D. Rendell[9], C. Reux[4], G. Rewoldt[80], T.T. Ribeiro[16], V. Riccardo[9], D. Richards[9], F. Rigollet[4], F.G. Rimini[64], L. Rios[15], M. Riva[19], J.E.C. Roberts[9], R.J. Robins[9], D.S. Robinson[9], S.A. Robinson[9], D.W. Robson[9], H. Roche[4], M. Rödig[44], N. Rodionov[12], V. Rohde[22], A. Rolfe[9], M. Romanelli[9], F. Romanelli[33,19], A. Romano[19], J. Romero[15], E. Ronchi[18], S. Rosanvallon[4], Ch. Roux[4], S. Rowe[9], M. Rubel[34], G. Rubinacci[10], M. Ruiz[57], C. Ruset[21], M. Russell[9], A. Ruth[24], L. Ryc[36], A. Rydzy[19], J. Rzadkiewicz[36], S. Saarelma[9], F. Sabathier[4], R. Sabot[4], S. Sadakov[30], A. Sadvakassova[51], A. Sadykov[51], P. Sagar[9], G. Saibene[25], A. Saille[4], F. Saint-Laurent[4], M. Salewski[85], A. Salmi[6], F. Salzedas[16], U. Samm[30], P. Sanchez[15], S. Sanders[9], S.G. Sanders[9], G. Sandford[9], K. Sandland[9], P. Sandquist[17], D.E.G. Sands[9], M.I.K. Santala[7], P. Santra[55], F. Sartori[25], R. Sartori[25], O. Sauter[38], A. Savelyev[2], A. Savtchkov[30], S.C. Scales[9], A. Scarabosio[22], N. Schaefer[4], V. Schmidt[13], A. Schmidt[30], O. Schmitz[30], S. Schmuck[86], M. Schneider[4], M. Scholz[36], K. Schöpf[67], B. Schweer[30], J. Schweinzer[22], M. Seki[50], L. Semeraro[19], A. Semerok[95], G. Sergienko[30], M. Sertoli[22], M.M.J. Shannon[9], S.E. Sharapov[9], S.R. Shaw[9], A. Shevelev[2], B. Sieglin[22], R. Sievering[44], C.A. Silva[16], P.A. Simmons[9], A. Simonetto[28], D. Simpson[9], S.K. Sipilä[7], A.C.C. Sips[33,64], P. Sirén[6], A. Sirinelli[9], H. Sjöstrand[18], D. Skopintsev[12], K. Slabkowska[36], P.G. Smith[9], J. Snipes[80], L. Snoj[82], S. Snyder[29], S. Soare[20], E.R. Solano[15], A. Soleto[15], W. Solomon[45], C. Soltane[4,33], P. Sonato[13], A. Sopplesa[13], A. Sorrentino[10], J. Sousa[16], C.B.C. Sowden[9], C. Sozzi[28], P. Späh[32], T. Spelzini[9], J. Spence[9], F. Spineanu[21], P. Spuig[4], R.D. Stagg[9], M.F. Stamp[9], V. Stancalie[21], P. Stangeby[46], R. Stankiewicz[36], C. Stan-Sion[91], D.E. Starkey[9], M.J. Stead[9], M. Stejner[85], A.V. Stephen[9], M. Stephen[55], A.L. Stevens[9], R.B. Stokes[9], D. Stork[9], D. Stoyanov[61], J. Strachan[45], P. Strand[17], M. Stransky[17], D. Strauss[32], D. Strintzi[78], W. Studholme[9], Y. Su Na[69], F. Subba[93], H.P. Summers[92], Y. Sun[30], C. Surdu-Bob[21], E. Surrey[9], D.J. Sutton[9], J. Svensson[86], D. Swain[31], B.D. Syme[9], I.D. Symonds[9], T. Szabolics[54], T. Szepesi[54], A. Szydlowski[36], F. Tabares[15], V. Takalo[96], H. Takenaga[50], T. Tala[6], A.R. Talbot[9], C. Taliercio[13], C.

Tame[9], M. Tardocchi[28], L. Taroni[13], G. Telesca[52], A. Terra[30], A.O. Terrington[9], D. Testa[38], J.M. Theis[4], J.D. Thomas[9], P.D. Thomas[9], P.R. Thomas[25], V.K. Thompson[9], C. Thomser[30], A. Thyagaraja[9], P.A. Tigwell[9], I. Tiseanu[21], R. Tivey[33,64], J.M. Todd[9], T.N. Todd[9], M.Z. Tokar[30], S. Tosti[19], P. Trabuc[4], J.M. Travere[4], P. Trimble[9], A. Trkov[82], E. Trukhina[11], M. Tsalas[58,65], E. Tsitrone[4], D. Tskhakaya jun[67], O. Tudisco[19], S. Tugarinov[12], M.M. Turner[24], S.G.J. Tyrrell[9], N. Umeda[50], B. Unterberg[30], H. Urano[50], A.J. Urquhart[9], I. Uytdenhouwen[42], A. Vaccaro[32], A.P. Vadgama[9], G. Vagliasindi[19], D. Valcarcel[16], M. Valisa[13], J. Vallory[4], M. Valovic[9], D. Van Eester[53], B. van Milligen[15], G.J. van Rooij[58], C.A.F. Varandas[16], S. Vartanian[4], K. Vasava[55], V. Vdovin[11], J. Vega[15], G. Verdoolaege[52], J.M. Verger[4], L. Vermare[4], C. Verona[14], Th. Versloot[58], M. Vervier[53], J. Vicente[16], S. Villari[19], E. Villedieu[4], F. Villone[10], J.E. Vince[9], G.J. Vine[9], I. Vinyar[84], B. Viola[10], E. Vitale[19], R. Vitelli[14], A. Vitins[26], M. Vlad[21], I. Voitsekhovitch[9], M. Vrancken[53], K. Vulliez[4], C.W.F. Waldon[9], M. Walker[9], M.J. Walsh[9], J. Waterhouse[9], M.L. Watkins[9,33], M.J. Watson[9], T. Wauters[4,53], M.W. Way[9], C.R. Webb[9], J. Weiland[17], H. Weisen[38,33], M. Weiszflog[18], R. Wenninger[22], A.T. West[9], J.M. Weulersse[95], M.R. Wheatley[9], A.D. Whiteford[92], A.M. Whitehead[9], A.G. Whitehurst[9], A.M. Widdowson[9], C. Wiegmann[30], S. Wiesen[30], A. Wilson[9], D. Wilson[9], D.J. Wilson[9], H.R. Wilson[97], M. Wischmeier[22], D.M. Witts[9], R.C. Wolf[30], J. Wolowski[36], P. Woscov[80], J. Wright[80], G.S. Xu[66], V. Yavorskij[67], V. Yerashok[40], M. Yoo[69], J. Yorkshades[9], C. Young[9], D. Young[9], I.D. Young[9], X. Yuhong[53], S. Yun[81], L. Zabeo[9], W. Zabolotny[36], L. Zaccarian[19], R. Zagorski[90,36], F.S. Zaitsev[88,83], L. Zakharov[45], R. Zanino[93], V. Zaroschi[21], K.D. Zastrow[9], I. Zatz[45], B. Zefran[82], W. Zeidner[22], M. Zerbini[19], T. Zhang[30], A. Zhitlukin[12], Y. Zhu[66], O. Zimmermann[30], V. Zoita[33,21], S. Zoletnik[54], W. Zwingman[4],

[1] Imperial College, University of London, London, SW7 2AZ, UK

[2] Ioffe Physico-Technical Institute, 26 Politekhnicheskaya, St Petersburg 194021, Russian Federation

[3] Association EURATOM-IPP.CR, Institute of Plasma Physics AS CR, Za Slovankou 3, 182 21 Praha 8, Czech Republic[4]Association EURATOM-CEA, CEA/DSM/IRFM, Cadarache 13108 Saint Paul Lez Durance, France

[5] Department of Pure and Applied Physics, Queens University, Belfast, BT7 1NN, UK

[6] VTT Technical Research Centre of Finland, Association EURATOM-Tekes, P.O.Box 1000, FIN-02044 VTT, Finland

[7] Aalto University, Association EURATOM-Tekes, P.O.Box 14100, FIN-00076 Aalto, Finland

[8] University of Tartu, Ülikooli 18, 50090 Tartu, Estonia

[9] Euratom/CCFE Fusion Association, Culham Science Centre, Abingdon, Oxon, OX14 3DB, UK

[10] Associazione EURATOM-ENEA sulla Fusione, Consorzio CREATE, Via Claudio 21, 80125 Napoli, Italy

[11] NRC Kurchatov Institute, 1 Kurchatov Square, Moscow 123182, Russian Federation

[12]Troitsk Insitute of Innovating and Thermonuclear Research (TRINITI), Troitsk 142190, Moscow Region, Russian Federation

[13] Associazione EURATOM-ENEA sulla Fusione, Consorzio RFX Padova, Italy
[14] Associazione EURATOM-ENEA sulla Fusione, Università di Roma, Italy
[15] Laboratorio Nacional de Fusion, Asociacion EURATOM-CIEMAT, Madrid, Spain
[16] Associação EURATOM/IST, Instituto de Plasmas e Fusão Nuclear, Instituto Superior Técnico, Av Rovisco Pais, 1049-001 Lisbon, Portugal
[17] Association EURATOM-VR, Department of Earth and Space Sciences, Chalmers University of Technology, SE-41296 Gothenburg, Sweden
[18] Association EURATOM-VR, Department of Physics and Astronomy, Uppsala University, SE-75120 Uppsala, Sweden
[19] Associazione EURATOM-ENEA sulla Fusione, C.R. Frascati, Roma, Italy
[20] The National Institute for Cryogenics and Isotopic Technology, Association EURATOM-MEdC, Ramnicu Valcea, Romania
[21] The National Institute for Laser, Plasma and Radiation Physics, Association EURATOM-MEdC, Magurele-Bucharest, Romania
[22] Max-Planck-Institut für Plasmaphysik, EURATOM-Assoziation, D-85748 Garching, Germany
[23] Dipartimento di Ingegneria Elettrica Elettronica e dei Sistemi-Università degli Studi di Catania, 95125 Catania, Italy
[24] Dublin City University (DCU), Ireland
[25] Fusion for Energy Joint Undertaking, Josep Pl. 2, Torres Diagonal Litoral B3, 08019, Barcelona, Spain
[26] University of Latvia, 19 Raina Blvd., Riga, LV 1586, Latvia
[27] The Nuclear Fuel Plant, Pitesti, Romania
[28] IFP-CNR, EURATOM-ENEA-CNR Association on Fusion, via R. Cozzi 53, 20125 Milano, Italy
[29] Lehigh University, Bethlehem, PA 18015, Pennsylvania, USA
[30] Forschungszentrum Jülich, Institute of Energy Research - Plasma Physics, EURATOM Association, D-52425, Jülich, Germany
[31] Oak Ridge National Laboratory, Oak Ridge, TN 37831-6169, Tennessee, USA
[32] Karlsruhe Institute of Technology, P.O.Box 3640, D-76021 Karlsruhe, Germany
[33] EFDA Close Support Unit, Culham Science Centre, Culham, OX14 3DB, UK
[34] Association EURATOM-VR, Fusion Plasma Physics, EES, KTH, SE-10044 Stockholm, Sweden
[35] University of Texas at Austin, Institute for Fusion Studies, Austin, TX 78712, Texas, USA
[36] Association Euratom-IPPLM, Hery 23, 01-497 Warsaw, Poland
[37] University of Helsinki, Association EURATOM-Tekes, P.O. Box 43, FI-00014 University of Helsinki, Finland
[38] Association EURATOM-Confédération Suisse, Ecole Polytechnique Fédérale de Lausanne (EPFL), CRPP, CH-1015 Lausanne, Switzerland

[39] Laboratoire J.A.Dieudonné, Université de Nice-Sophia-Antipolis, Parc Valrose, F-06108 Nice CEDEX 02, France
[40] Magnetic Sensor Laboratory (LPNU), 1 Kotliarevsky Str, Lviv, 79013, Ukraine
[41] University Milano-Bicocca, EURATOM-ENEA-CNR Association on Fusion, piazza della Scienza 3, 20126 Milano, Italy
[42] Association EURATOM-SCK-CEN, Nuclear Research Centre, 2400 Mol, Belgium
[43] The National Institute for Optoelectronics, Magurele-Bucharest, Romania, Association EURATOM-MEdC
[44] Forschungszentrum Jülich, Institute of Energy Research, EURATOM Association, D-52425, Jülich, Germany
[45] Princeton Plasma Physics Laboratory, James Forrestal Campus, Princeton, NJ 08543, New Jersey, USA
[46] General Atomics, P.O.Box 85608, San Diego, CA 92186-5608, California, USA
[47] Department of Electrical and Electronic Engineering, University of Cagliari, Piazza d'Armi 09123 Cagliari, Italy
[48] University of California, 1111 Franklin St., Oakland, CA 94607, USA
[49] Colorado School of Mines, 1500 Illinois Street, Golden, CO 80401, Colorado, USA
[50] Japan Atomic Energy Agency, Naka Fusion Research Establishment, Nakamachi, Naka-gun, Ibaraki-ken 311-0913, Japan
[51] ASE Institute of Atomic Energy, RSE NNC RK, Krasnoarmeyskaya 10, Kurchatov, V-Kazakhstanskaya, Kazakhstan
[52] Department of Applied Physics UG (Ghent University) St-Pietersnieuwstraat 41 B-9000 Ghent Belgium
[53] Association "EURATOM - Belgian State" Laboratory for Plasma Physics Koninklijke Militaire School - Ecole Royale Militaire Renaissancelaan 30 Avenue de la Renaissance B-1000 Brussels Belgium
[54] Association EURATOM/HAS, Wigner Research Centre for Physics, P.O.B. 49, H - 1525 BUDAPEST
[55] Institute for Plasma Research, Bhat, Gandhinagar - 382 428, Gujarat State, India
[56] CEA/Fontenay aux Roses, B.P.6 F-92265 Fontenay-aux-roses CEDEX, France
[57] Universidad Politécnica de Madrid, Grupo I2A2, Madrid, Spain
[58] FOM Institute DIFFER P.O. Box 1207 NL-3430 BE Nieuwegein, The Netherlands
[59] Institute of Applied Physics, Nizhny Novgorod 603155, Russian Federation
[60] University of California, San Diego, 9500 Gilman drive, La Jolla, CA 92093, United States
[61] Association EURATOM-INRNE Institute of Elecronics, Bulgarian Academy of Sciences, 72 Tzarigradsko shosse, Sofia 1784, Bulgaria
[62] Association EURATOM-VR, Department of Material Physics, ICT, KTH, SE-16440 Kista, Sweden

[63] Association EURATOM-HAS, Budapest Univeristy of Technology and Economics, H-1111 Budapest, Hungary
[64] European Commission, B-1049 Brussels, Belgium
[65] Association EURATOM-Hellenic Republic, NCSR "Demokritos" 153 10, Agia Paraskevi Attikis, Greece
[66] Institute of Plasma Physics, Chinese Academy of Sciences, Hefei, 230031, China
[67] University of Innsbruck, Association EURATOM-Österreichische Akademie der Wissenschaften (ÖAW), Austria
[68] Institute for Plasma Research, University of Maryland, College Park, MD 20742-3511, Maryland, USA
[69] Seoul National University, Shilim-Dong, Gwanak-Gu, Republic of Korea
[70] ITER Organization, Route de Vinon, CS 90 046, 13067 Saint Paul Lez Durance, France
[71] 291 Daehak-ro(373-1 Guseong-dong), Yuseong-gu, Daejeon 305-701, Republic of Korea
[72] Daegu University, Jillyang, Gyeongsan, Gyeongbuk 712-174, Republic of Korea
[73] Association EURATOM-LEI, Breslaujos str. 3, LT-44403, Kaunas, Lithuania
[74] Association EURATOM-VR, Department of Physics, Lund University, SE-22100 Lund, Sweden
[75] Association EURATOM-VR, Department of Engineering Sciences, Uppsala University, SE-75120 Uppsala, Sweden
[76] Vienna University of Technology, Association EURATOM-Österreichische Akademie der Wissenschaften (ÖAW), Austria
[77] Physics Section, Division of Physical and Chemical Sciences, International Atomic Energy Agency, P.O. Box 100, Wagramer Strasse 5, A-1400 Vienna, Austria
[78] Association EURATOM-Hellenic Republic, National Technical University of Athens, Iroon Politechniou 9, 157 73 Zografou, Athens, Greece
[79] IPF, Stuttgart University, Stuttgart, Germany
[80] MIT Plasma Science and Fusion Centre, Cambridge, MA 02139, Massachusetts, USA
[81] Gwahangno 169-148 (Eoeun-dong), Yusung-gu, Daejeon, Korea 305-806
[82] Association EURATOM-MHST, Jozef Stefan Institute, Reactor Physics Department, Jamova 39, SI-1000 Ljubljana, Slovenia
[83] Moscow State University, Moscow 119991, Russian Federation
[84] 27a, Gzhatskaya Ulitsa, Saint Petersburg, 195220, Russia
[85] Association EURATOM-DTU, Technical University of Denmark, Department of Physics, DTU Risø Campus, P.O.Box 49, DK-4000 Roskilde, Denmark
[86] Max-Planck-Institut für Plasmaphysik, Teilinsitut Greifswald, EURATOM-Assoziation, D-17491 Greifswald, Germany
[87] Departamento de Física, Universidad Carlos III de Madrid, 28911 Leganés, Madrid, Spain
[88] Department of Experimental Physics, Faculty of Mathematics, Physics and Informatics

Comenius University Mlynska dolina F2, 84248 Bratislava, Slovak Republic
[89] Association EURATOM-VR, Department of Physics, SCI, KTH, SE-10691 Stockholm, Sweden
[90] EFDA Close Support Unit, D-85748 Garching, Germany
[91] The “Horia Hulubei” National Institute for Physics and Nuclear Engineering, Association EURATOM-MEdC, Magurele-Bucharest, Romania
[92] Department of Physics and Applied Physics, University of Strathclyde, Glasgow, G4 ONG, UK
[93] Associazione EURATOM-ENEA sulla Fusione, Politecnico di Torino, Italy
[94] Department of Physics, University of Warwick, Coventry, CV4 7AL, UK
[95] CEA/Saclay, F-91191 Gif-sur-Yvette CEDEX, France
[96] Tampere University of Technology, Association EURATOM-Tekes, P.O. Box 527, FI-33101 Tampere, Finland
[97] University of York, Heslington, York YO10 5DD, UK